Mathematical Biosciences and Engineering

https://www.aimspress.com/journal/mbe

MBE, 21(3): 4521–4553.
DOI: 10.3934/mbe.2024200
Received: 10 December 2023
Revised: 09 January 2024
Accepted: 17 January 2024
Published: 28 February 2024

Research article

Nonlocal delay gives rise to vegetation patterns in a vegetation-sand model

Jichun Li*, Gaihui Guo and Hailong Yuan

School of Mathematics and Data Science, Shaanxi University of Science and Technology, Xi'an 710021, China

* **Correspondence:** Email: 2820700251@qq.com.

Abstract: The vegetation pattern generated by aeolian sand movements is a typical type of vegetation patterns in arid and semi-arid areas. This paper presents a vegetation-sand model with nonlocal interaction characterized by an integral term with a kernel function. The instability of the Turing pattern was analyzed and the conditions of stable pattern occurrence were obtained. At the same time, the multiple scales method was applied to obtain the amplitude equations at the critical value of Turing bifurcation. The spatial distributions of vegetation under different delays were obtained by numerical simulation. The results revealed that the vegetation biomass increased as the interaction intensity decreased or as the nonlocal interaction distance increased. We demonstrated that the nonlocal interaction between vegetation and sand is a crucial mechanism for forming vegetation patterns, which provides a theoretical basis for preserving and restoring vegetation.

Keywords: vegetation-sand model; nonlocal delay; multiple scale analysis; amplitude equation

1. Introduction

Desertification is land degradation in dry semi-humid arid, semi-arid, and arid areas resulting from various factors, including climatic variation and human activities [1]. This process can bring about significant negative consequences for society and the economy, which include reduced agricultural output, destruction of property, and heightened health and safety risks [2, 3]. Numerous ecosystems in arid and semi-arid regions are experiencing accelerated desertification [4, 5]. In areas with frequent movement of sand caused by wind, desertification is primarily attributed to the displacement of sand, which leads to the depletion of vegetation cover [6, 7].

However, regarding the research on vegetation modeling, more scholars focus on vegetation water modeling and less on vegetation-sand modeling. They believe that rainfall rate can induce transitions among bare soil state, vegetation pattern state, and homogeneous vegetation state [8–11]. In 1999, Klausmeier [12] first proposed a model with two variables, vegetation biomass and water density, for

forming regular vegetation patterns in semi-arid areas. The results showed that the regularity of vegetation patterns in semi-arid regions is the traveling wave instability of the reaction-diffusion convection equation. The proposed model has facilitated the study of vegetation patterns in semi-arid areas. Meron et al. [13] presented a continuum model for vegetation patterns in water-limited systems. The model predicted transitions from bare soil at low precipitation to homogeneous vegetation at high rainfall through intermediate states of spot, stripe, and gap patterns.

In the past century, with significant growth and widespread occurrence of soil desertification and numerous sand transport and deposition events, the relevance of aeolian sand as a significant environmental concern has only emerged in the last two decades [14]. There is a growing recognition among people that vegetation patch formation using wind as a driver is important when dealing with environmental issues [15–19]. Zhang et al. [20] presented a model based on the two variables of vegetation cover and the height of aeolian sand accumulation

$$\begin{cases} \dfrac{\partial S}{\partial T} = K_0 + MV(1 - \dfrac{V}{V_0}) - NS - A_1\dfrac{\partial S}{\partial X} + D_1(\dfrac{\partial^2 S}{\partial X^2} + \dfrac{\partial^2 S}{\partial Y^2}), \\ \dfrac{\partial V}{\partial T} = HV(1 - \dfrac{V}{Vm}) - PS\dfrac{V}{C+V} - A_2\dfrac{\partial V}{\partial X} + D_2(\dfrac{\partial^2 V}{\partial X^2} + \dfrac{\partial^2 V}{\partial Y^2}), \end{cases}$$

where $\frac{\partial S}{\partial T}$ and $\frac{\partial V}{\partial T}$ are the accumulation rate of sand and the growth rate of vegetation respectively, $K_0 + MV(1 - \frac{V}{V_0}) - NS$ represents deposition by vegetation, $A_1\frac{\partial S}{\partial X}$ and $A_2\frac{\partial V}{\partial X}$ represent advection by prevailing wind and dispersal by prevailing wind respectively, $HV(1-\frac{V}{Vm})$ is vegetation growth, $PS\frac{V}{C+V}$ represents vegetation destroyed by sand, and $D_1(\frac{\partial^2 S}{\partial X^2} + \frac{\partial^2 S}{\partial Y^2})$ and $D_2(\frac{\partial^2 V}{\partial X^2} + \frac{\partial^2 V}{\partial Y^2})$ represent sand diffusion in all directions and dispersal in all directions respectively.

Zhang et al. [20] studied the effect of wind-sand on the spatial distribution of vegetation in the windy sand environment. The influence of the prevailing wind on the growth rate of the two variables is modeled as an advection term in the model, while the effect of other winds is modeled as a diffusion term. Many areas may not have significant prevailing winds. We can obtain the following model

$$\begin{cases} \dfrac{\partial S}{\partial T} = K_0 + MV(1 - \dfrac{V}{V_0}) - NS + D_1(\dfrac{\partial^2 S}{\partial X^2} + \dfrac{\partial^2 S}{\partial Y^2}), \\ \dfrac{\partial V}{\partial T} = HV(1 - \dfrac{V}{Vm}) - PS\dfrac{V}{C+V} + D_2(\dfrac{\partial^2 V}{\partial X^2} + \dfrac{\partial^2 V}{\partial Y^2}). \end{cases} \tag{1.1}$$

Zhang et al. [20] considered that the aggregation effect of vegetation on sand decreases with the increase of vegetation biomass. Different from Zhang et al. [20], this paper considers the mechanism of aggregation effect of the linear action term, and the model (1.1) can be rewritten as follows

$$\begin{cases} \dfrac{\partial S}{\partial T} = K_0 + MV - NS + D_1\Delta S, \\ \dfrac{\partial V}{\partial T} = HV(1 - \dfrac{V}{Vm}) - PS\dfrac{V}{C+V} + D_2\Delta V. \end{cases} \tag{1.2}$$

For ease of analysis, let

$$s = \frac{N}{K_0}S, \quad v = \frac{M}{K_0}V, \quad t = NT, \quad h = \frac{H}{N}, \quad v_m = \frac{MV_m}{K_0}, \quad p = \frac{PK_0}{CN^2},$$

$$c = \frac{K_0}{CM}, \quad d = \frac{D_2}{D_1}, \quad x = \sqrt{\frac{N}{D_1}}X, \quad y = \sqrt{\frac{N}{D_1}}Y.$$

The dimensionless system (1.2) is obtained as follows

$$\begin{cases} \dfrac{\partial s}{\partial t} = 1 + v - s + \Delta s, \\ \dfrac{\partial v}{\partial t} = hv(1 - \dfrac{v}{v_m}) - ps\dfrac{v}{1 + cv} + d\Delta v, \end{cases} \tag{1.3}$$

where s and v are the height of the sand accumulation layer and vegetation coverage respectively, h describes the intrinsic growth rate of vegetation cover, v_m represents the potential maximum value of vegetation coverage, p is the coefficient of destructive effects by sand burial, c is the half-saturation constant of sand capacity, d denotes the ratio of the diffusivity of vegetation to that of sand, the term $ps\frac{v}{1+cv}$ models local destruction of vegetation by sand, and Δ is a standard Laplace operator. The vegetation-sand system reflects the influence of sand on vegetation.

Nonlocal interaction is one of the critical mechanisms of vegetation pattern formation. Many scholars have researched the nonlocal effects of vegetation models [21–25]. However, no one has yet studied the nonlocal interaction of sand and vegetation. Fine aeolian sand particles are deposited on the surface of leaves and stems, which will affect the life process of vegetation photosynthesis to a certain extent, and the deposited sand will reduce the water content of the soil and inhibit the growth of vegetation. In addition to the location of the vegetation itself, the aeolian sand in the vicinity and even the whole study area will destroy the development of the foliage. During the transportation of the aeolian sand, it will impact and abrase the stems and leaves of the vegetation, directly damaging the vegetation tissue and affecting its productivity. The accumulation of a large amount of aeolian sand may even bury the vegetation. Hence, it is interesting to study the nonlocal interaction between vegetation and sand. This paper introduces a nonlocal interaction in model (2.1) to better account for the effect of aeolian sand on vegetation growth throughout the study area.

In reality, time delays are inevitable and substantially impact the dynamics [26–30]. It takes time for sand to be transported by wind to destroy vegetation, which shows that in the spatial scope of our study, the whole process of vegetation destroyed by sand will be affected by nonlocal effects and time delay. In the modelling of complex systems portraying vegetation-sand interactions, the spatially weighted average of nonlocal delay including the entire study area, first proposed by Britton, can be used to solve the problem that the study object is not at the current location of the study area at the current moment at the previous moments [31]. This reaction-diffusion equation with delay including a spatially weighted average over the entire study region is called the nonlocal reaction-diffusion equation. Nonlocal reaction-diffusion equations have been widely used in the fields of infectious diseases and predation by predation among animals, but in the field of eco-vegetation most of them are focused on the study of local and global existence and asymptotic approximation of the model solutions, as well as wavefront solutions and periodic wavefront solutions [32–37]. The use of nonlocal delay reaction-diffusion equations to study the vegetation patchwork in arid and semi-arid regions is a new research direction in ecological vegetation science, which can truly portray the actual situation of nonlocal action of vegetation [38–43], and its theory about combating desertification still needs to be improved. Therefore, this paper establishes a vegetation-sand model with nonlocal effects in arid and semi arid regions, analyzes the model for Turing instability, reveals the influence of vegetation model

parameters on vegetation patchwork, and provides theoretical basis for specific measures to combat land desertification.

Studying the effect of aeolian sand diffusion intensity on vegetation is the main objective of this paper, which compares the effect of two mechanisms on changes in vegetation pattern structure based on nonlocal delays. The rest of this paper is organized as follows. Section 2 derives a nonlocal delayed vegetation-sand model with soil-sand diffusion. Section 3 discusses the stability of the equilibria and the conditions for the emergence of the Turing pattern. We address a weakly nonlinear multiple scales analysis and obtain the amplitude equation for the Turing pattern in Section 4. In Section 5, numerical simulations are shown to verify the theoretical results.

2. A mathematical model derivation

In semi-arid environments, vegetation and sand produce nonlocal interaction. In addition to the vegetation-covered areas, aeolian sand will have corresponding impacts on the vegetation throughout the study area. It will erode stems and leaves, damage plant tissues, and affect their productivity, among other things. To better describe the process, we create the following vegetation-sand system with nonlocal delay

$$\begin{cases} \dfrac{\partial s(x,y,t)}{\partial t} = 1 + v - s + \nabla^2 s, & (x,y) \in \Omega,\ t > 0, \\ \dfrac{\partial v(x,y,t)}{\partial t} = hv(1 - \dfrac{v}{v_m}) + d\nabla^2 v & (x,y) \in \Omega,\ t > 0, \\ \qquad\qquad - p\int_\Omega \int_{-\infty}^{t} Q(x,y,t-U)H(t-U)s(y,U)\mathrm{d}U\mathrm{d}y\dfrac{v}{1+cv}, & \\ \dfrac{\partial s(x,y,t)}{\partial \nu} = \dfrac{\partial v(x,y,t)}{\partial \nu} = 0, & (x,y) \in \partial\Omega,\ t > 0, \\ s(x,y,0) \geq 0,\quad v(x,y,0) \geq 0, & (x,y) \in \bar{\Omega}. \end{cases} \tag{2.1}$$

For a detailed explanation of the kernel function [44, 45]

$$f(t) = \delta(t-\tau), \quad f(t) = \frac{1}{\tau}e^{-\frac{t}{\tau}}, \quad f(t) = \frac{1}{\tau^2}e^{-\frac{t}{\tau}}.$$

The second and third of the above three kernels are referred to as weak and strong generic delay kernels respectively. The first kernel is the appropriate choice for giving a model with a discrete time delay, that is to say, the delay effect only involves the data exactly τ time units ago, $H(t)$ is the weak generic delay kernel for the Neumann problem and the expression is as follows

$$H(t) = \frac{1}{\tau}e^{-\frac{t}{\tau}}.$$

The kernel function $Q(x,y,t)H(t)$ represents the weight of eolian sand reaching the current position at any position before time t. The expression of nonlocal delay is as follows

$$\begin{aligned} n(x,t) &= \int_\Omega \int_{-\infty}^{t} Q(x,y,t-U)H(t-U)s(y,U)\mathrm{d}U\mathrm{d}y \\ &= \int_\Omega \int_{-\infty}^{t} Q(x,y,t-U)\frac{1}{\tau}e^{-\frac{t-U}{\tau}}s(y,U)\mathrm{d}U\mathrm{d}y. \end{aligned}$$

$Q(x, y, t)$ is the solution of the following system in a bounded domain

$$\begin{cases} \dfrac{\partial Q}{\partial t} = D\Big(\dfrac{\partial^2 Q}{\partial X^2} + \dfrac{\partial^2 Q}{\partial Y^2}\Big), & X \times Y \in \Omega,\ t > 0, \\ \dfrac{\partial Q}{\partial \nu}\Big|_{\partial\Omega} = 0, & t > 0, \\ Q(x, y, 0) = \sigma(x - y) = \sigma(y - x), & x, y \in \Omega \end{cases} \tag{2.2}$$

and

$$\begin{aligned} \frac{\partial n}{\partial t} =& \int_\Omega \frac{1}{\tau} Q(x, y, 0) s(y, t) \mathrm{d}y \\ &+ \int_\Omega \int_{-\infty}^{t} \frac{1}{\tau} s(y, h) \Big[\frac{\partial Q(x, y, t - U)}{\partial t} e^{-\frac{t-U}{\tau}} - \frac{1}{\tau} Q(x, y, t - U) e^{-\frac{t-U}{\tau}} \Big] \mathrm{d}U \mathrm{d}y \\ =& \int_\Omega \frac{1}{\tau} \sigma(x - y) s(y, t) \mathrm{d}y \\ &+ \int_\Omega \int_{-\infty}^{t} \frac{1}{\tau} s(y, U) e^{-\frac{t-U}{\tau}} \Big[\frac{\partial Q(x, y, t - U)}{\partial t} - \frac{1}{\tau} Q(x, y, t - U) \Big] \mathrm{d}U \mathrm{d}y, \end{aligned}$$

where σ is the Dirac delta function and $D > 0$. According to (2.2) and the properties of σ function, the above equation can be derived as follows

$$\begin{aligned} \frac{\partial n}{\partial t} =& \frac{1}{\tau} \Big[s(x, t) - \int_\Omega \int_{-\infty}^{t} \frac{1}{\tau} e^{-\frac{t-U}{\tau}} s(y, U) Q(x, y, t - U) \mathrm{d}U \mathrm{d}y \Big] \\ &+ D \int_\Omega \int_{-\infty}^{t} \Big(\frac{\partial^2 Q(x, y, t - U)}{\partial X^2} + \frac{\partial^2 Q(x, y, t - U)}{\partial Y^2} \Big) \frac{1}{\tau} e^{-\frac{t-U}{\tau}} s(y, U) \mathrm{d}U \mathrm{d}y \\ =& \frac{1}{\tau}(s - n) + D\nabla^2 n. \end{aligned}$$

Based on the above derivation, (2.1) can be transformed into the following form

$$\begin{cases} \dfrac{\partial s}{\partial t} = 1 + v - s + \nabla^2 s, & x \in \Omega,\ t > 0, \\ \dfrac{\partial v}{\partial t} = hv(1 - \dfrac{v}{v_m}) - pn\dfrac{v}{1 + cv} + d\nabla^2 v, & x \in \Omega,\ t > 0, \\ \dfrac{\partial n}{\partial t} = \dfrac{1}{\tau}(s - n) + D\nabla^2 n, & x \in \Omega,\ t > 0, \\ \dfrac{\partial s(x, t)}{\partial \nu} = \dfrac{\partial v(x, t)}{\partial \nu} = \dfrac{\partial n(x, t)}{\partial \nu} = 0, & x \in \partial\Omega,\ t > 0, \\ s(x, 0) = s_0(x) \geq 0, \not\equiv 0, \quad v(x, 0) = v_0(x) \geq 0, \not\equiv 0, & \\ n(x, 0) = n_0(x) \geq 0, \not\equiv 0, & x \in \bar{\Omega}. \end{cases} \tag{2.3}$$

System (1.3) always has one bare sand state equilibrium point $K_0 = (1, 0)$. When $v \neq 0$, we have

$$-\frac{ch}{v_m} v^2 + (ch - p - \frac{h}{v_m}) v + h - p = 0. \tag{2.4}$$

Let

$$A = -\frac{ch}{v_m} < 0, \quad B = ch - p - \frac{h}{v_m}, \quad C = h - p.$$

The number of equilibrium points in system (1.3) depends on the relationship between above parameters.

(i) When the parameters satisfy the condition $B^2 - 4AC > 0, B - \sqrt{B^2 - 4AC} > 0$, Eq (2.4) has two positive roots

$$v_{11} = \frac{-B + \sqrt{B^2 - 4AC}}{2A}, \quad v_{12} = \frac{-B - \sqrt{B^2 - 4AC}}{2A}.$$

Therefore, there are $s_{11} = 1 + v_{11},\ s_{12} = 1 + v_{12}$. It can be obtained that system (1.3) has two uniformly vegetated equilibrium points $K_{11} = (s_{11}, v_{11}),\ K_{12} = (s_{12}, v_{12})$.

(ii) When the parameters satisfy the condition $B^2 - 4AC = 0, B > 0$, Eq (2.4) has a unique positive root, $v_2 = -\frac{B}{2A}$ and $s_2 = 1 + v_2$. Therefore, system (1.3) has an equilibrium point $K_2 = (s_2, v_2)$.

(iii) When the parameters satisfy the condition $B^2 - 4AC < 0$, Eq (2.4) does not have any real roots, indicating that there is no equilibrium for system (1.3).

In order to discuss the stability of the above equilibrium point, system (1.3) is linearized near the equilibrium point $K^* = (s_*, v_*)$ to obtain the Jacobin matrix

$$J = \begin{pmatrix} -1 & 1 \\ -\dfrac{pv_*}{1+cv_*} & h - \dfrac{2hv_*}{v_m} - \dfrac{ps_*}{(1+cv_*)^2} \end{pmatrix} = \begin{pmatrix} -1 & 1 \\ -N & H \end{pmatrix}.$$

Let $H = h - \dfrac{2hv_*}{v_m} - \dfrac{ps_*}{(1+cv_*)^2}, N = \dfrac{pv_*}{1+cv_*}$. Its corresponding characteristic equation is

$$\mu^2 - \mathrm{Tr}J\mu + \mathrm{Det}J = 0,$$

where

$$\mathrm{Tr}J = H - 1, \qquad \mathrm{Det}J = N - H.$$

We can see that if $H < 1$ and $H < N$, then the equilibrium (s_*, v_*) is locally asymptotically stable for (1.3). The following discussions are all assumed that $H < 1$ and $H < N$.

3. Linear analysis and Turing patterns

3.1. Stability and Turing bifurcation analysis of the diffusive system without nonlocal delay

In this subsection, we study (1.3) without considering the nonlocal delay. We start with the local system in one-dimensional space $\Omega = (0, \pi)$

$$\begin{cases} s_t = 1 + v - s + \nabla^2 s, & x \in (0,\pi), t > 0, \\ v_t = hv(1 - \dfrac{v}{v_m}) - ps\dfrac{v}{1+cv} + d\nabla^2 v, & x \in (0,\pi), t > 0, \\ s_x(x,t) = v_x(x,t) = 0, & x = 0, \pi, t > 0, \\ s(x,0) = s_0(x) \geq 0, v(x,0) = v_0(x) \geq 0, & x \in (0,\pi). \end{cases} \tag{3.1}$$

Define the real Sobolev space

$$X = \{(s, v) \in H^2(0,\pi) \times H^2(0,\pi) : (s_x, v_x)\,|_{x=0,\pi} = 0\},$$

and let the complex extension space of X:$X_C = X \bigoplus iX = \{x_1 + ix_2 \mid x_1, x_2 \in X\}$. The linearization operator for system (3.1) at (s_*, v_*) is

$$L = \begin{pmatrix} -1 + \nabla^2 & 1 \\ -N & H + \nabla^2 \end{pmatrix}.$$

Under the chi-square Neumann condition, the eigenvalue of operator $-\nabla^2$ is $\mu_k = k^2$ $(k = 0, 1, 2, \cdots)$, which satisfies

$$0 = \mu_0 < \mu_1 \leq \mu_2 \leq \mu_3 \leq \cdots,$$

and $\cos(kx)$ $(k \in N)$ corresponds to the characteristic function of μ_k. Taking the sequence of functions $\{\cos(kx)\}_{k=0}^{\infty}$, it is a standard Orthonormal basis of space $L^2(0, \pi)$.

Let

$$\begin{pmatrix} \phi \\ \varphi \end{pmatrix} = \sum_{k=0}^{\infty} \begin{pmatrix} a_k \\ b_k \end{pmatrix} \cos(kx)$$

be the eigenfunction of L corresponding to eigenvalue ψ, where $L(\phi, \varphi)^T = \psi(\phi, \varphi)^T$. By direct calculation, we have

$$L_k \begin{pmatrix} a_k \\ b_k \end{pmatrix} = \psi \begin{pmatrix} a_k \\ b_k \end{pmatrix}, \quad k = 0, 1, 2, \cdots$$

and

$$L_k = \begin{pmatrix} -1 - \mu_k & 1 \\ -N & H - d\mu_k \end{pmatrix}.$$

Let the characteristic equation of L_k be

$$\lambda^2 - T_k \lambda + D_k = 0, \tag{3.2}$$

where

$$T_k = H - 1 - (1 + d)\mu_k < 0, \qquad D_k = d\mu_k^2 + (d - H)\mu_k + N - H.$$

Obviously, when $H \leq 0$, for any $k \geq 0$, we have $D_k \geq 0$ and $T_k < 0$. At this point, the positive equilibrium point (s_*, v_*) of system (3.1) is locally asymptotically stable.

In the following, assume that $0 < H < 1$ and $H < N$. If $d \geq H$, then for any $k \geq 0$, we obviously have $D_k \geq 0$ and $T_k < 0$, which implies that (s_*, v_*) is locally asymptotically stable. If $d < H$, then let

$$\Delta = (d - H)^2 - 4(N - H)d = d^2 + (2H - 4N)d + H^2.$$

Note that the discriminant of the quadratic function $f(z) = z^2 + (2H - 4N)z + H^2$ is

$$\tilde{\Delta} = (2H - 4N)^2 - 4H^2 = 16N(N - H) > 0.$$

Thus, $f(z) = 0$ exists two positive real roots

$$z_1 = 2N - H - 2\sqrt{N(N - H)}, \quad z_2 = 2N - H + 2\sqrt{N(N - H)}.$$

If $z_1 < z < z_2$, then $f(z) < 0$ and $\Delta < 0$, which implies $D_k > 0$ for any $k > 0$ when $z_1 < d < z_2$. Let $z_1 - H = 2N - 2H - 2\sqrt{N(N - H)}$. Since $H < N$, $N - H < \sqrt{N}\sqrt{N - H}$. We can get $z_1 < H$. Obviously, $Z_2 > H$. Note that $z_1 < H < z_2$ and (s_*, v_*) is locally asymptotically stable when $d \geq H$. Hence, (s_*, v_*) is locally asymptotically stable when $d > z_1$.

Theorem 3.1. *Assume that $H < 1$ and $H < N$ hold. Then, the equilibrium point (s_*, v_*) is locally asymptotically stable for system (1.3) if $H \leq 0$. When $H > 0$, the equilibrium point (s_*, v_*) is locally asymptotically stable for system (1.3) if $d > z_1$, where $z_1 = 2N - H - 2\sqrt{N(N-H)} > 0$.*

If $0 < d < z_1$, then $\Delta > 0$. The equation

$$d\mu_k^2 + (d - H)\mu_k + N - H = 0$$

has two positive real roots

$$\mu_-(d) = \frac{H - d - \sqrt{(d-H)^2 - 4(N-H)d}}{2d}, \quad \mu_+(d) = \frac{H - d + \sqrt{(d-H)^2 - 4(N-H)d}}{2d}.$$

Let $F(d) = H - d + \sqrt{(d-H)^2 - 4(N-H)d}$. Then,

$$F'(d) = -1 + \frac{d + H - 2N}{\sqrt{(d-H)^2 - 4(N-H)d}}.$$

Recall that $H > z_1$ and $d < z_1$. It follows from $d < H < N$ that $d < 2N - H$. Hence, we can get $F'(d) < 0$ and $\mu_+(d)$ is monotonically decreasing on d.

Define

$$\Phi_1 = \{\mu \mid \mu \geq 0, \mu_-(d) < \mu < \mu_+(d)\}, \quad \Phi_2 = \{\mu_0, \mu_1, \mu_2, \mu_3, \cdots\}.$$

Let $d \to 0^+$. Then, we have

$$\lim_{d\to 0^+} \mu_-(d) = \frac{N-H}{N} > 0, \quad \lim_{d\to 0^+} \mu_+(d) = +\infty.$$

Clearly, we see that $\Phi_1 \cap \Phi_2 \neq \emptyset$, which implies that the positive equilibrium (s_*, v_*) of system (3.1) is unstable. So, we obtain the Turing instability of (s_*, v_*) for d is small.

Theorem 3.2. *Assume that $0 < H < 1$ and $H < N$ hold. Then, there exists sufficiently small $\tilde{d}$ such that for $0 < d < \tilde{d}$, the positive equilibrium (s_*, v_*) is Turing unstable for system (3.1).*

3.2. Stability analysis for the local system with nonlocal delay

In this section, we will study the conditions under which the equilibrium point (s_*, v_*, n_*) is stable when the system (2.3) has no diffusion.

Begin with the local system

$$\begin{cases} \dfrac{\mathrm{d}s}{\mathrm{d}t} = 1 + v - s, \\ \dfrac{\mathrm{d}v}{\mathrm{d}t} = hv(1 - \dfrac{v}{v_m}) - pn\dfrac{v}{1+cv}, \\ \dfrac{\mathrm{d}n}{\mathrm{d}t} = \dfrac{1}{\tau}(s - n), \end{cases} \tag{3.3}$$

where $t > 0$. The linearized system of (3.3) at equilibrium (s_*, v_*, n_*) is

$$\begin{cases} \dfrac{\mathrm{d}s}{\mathrm{d}t} = a_{11}s + a_{12}v + a_{13}n, \\ \dfrac{\mathrm{d}v}{\mathrm{d}t} = a_{21}s + a_{22}v + a_{23}n, \\ \dfrac{\mathrm{d}n}{\mathrm{d}t} = a_{31}s + a_{32}v + a_{33}n, \end{cases}$$

where

$$a_{11} = -1, \qquad a_{12} = 1, \qquad a_{13} = 0,$$
$$a_{21} = 0, \qquad a_{22} = h - \frac{2hv_*}{v_m} - \frac{pn_*}{(1+cv_*)^2}, \qquad a_{23} = -\frac{pv_*}{1+cv_*},$$
$$a_{31} = \frac{1}{\tau}, \qquad a_{32} = 0, \qquad a_{33} = -\frac{1}{\tau}.$$

We analyzed the stability of the equilibrium point (s_*, v_*, n_*) in Table 3-1 [46].

Table 3-1. Stability analysis of equilibrium point according to Hurwitz criterion.

Characteristic polynomial of system (3.2)	Stability condition
$\sigma^3 + P_1(0)\sigma^2 + P_2(0)\sigma + P_3(0) = 0$	$P_1(0) > 0$ $P_3(0) > 0$ $P_1(0)P_2(0) - P_3(0) > 0$

The coefficients in Table 3-1 are shown below

$$P_1(0) = -(a_{11} + a_{22} + a_{33}) = 1 + \frac{1}{\tau} - h + \frac{2hv_*}{v_m} + \frac{pn_*}{(1+cv_*)^2},$$

$$\begin{aligned} P_2(0) &= a_{11}a_{22} + a_{33}a_{22} + a_{11}a_{33} - a_{12}a_{21} - a_{13}a_{31} - a_{23}a_{32} \\ &= \frac{1}{\tau} + (1 + \frac{1}{\tau})(-h + \frac{2hv_*}{v_m} + \frac{pn_*}{(1+cv_*)^2}), \end{aligned}$$

$$\begin{aligned} P_3(0) &= a_{11}a_{23}a_{32} + a_{12}a_{21}a_{33} + a_{13}a_{22}a_{31} - a_{11}a_{22}a_{33} - a_{12}a_{23}a_{31} - a_{13}a_{21}a_{32} \\ &= \frac{1}{\tau}[-h + \frac{2hv_*}{v_m} + \frac{pv_*}{1+cv_*} + \frac{pn_*}{(1+cv_*)^2}]. \end{aligned}$$

Condition 1. When $H < 1$ and $H < N$, $P_1(0) > 0$ and $P_3(0) > 0$.

Condition 2. When $H < 1$ and $H < N$, $P_1(0)P_2(0) - P_3(0) > 0$.

$$\begin{aligned} P_1(0)P_2(0) - P_3(0) = (1 + \frac{1}{\tau})X_1^2 + (1 + \frac{1}{\tau})[1 + \frac{1}{\tau} + \frac{2p(1+\beta)}{(1+c\beta)^2}]X_1 - \frac{pc\beta^2 + 2p\beta + p}{\tau(1+c\beta)^2} \\ + [1 + \frac{1}{\tau} + \frac{p(1+\beta)}{(1+c\beta)^2}][\frac{1}{\tau} + (\frac{1}{\tau} + 1)\frac{p(1+\beta)}{(1+c\beta)^2}] > 0. \end{aligned}$$

Let $(s_*, v_*, n_*) = (1+\beta, \beta, 1+\beta)$ and $X_1 = \frac{2h\beta}{v_m} - h$. Then, we have

$$A_1X_1^2 + B_1X_1 + C_1 > 0,$$

$$A_1 = 1 + \frac{1}{\tau} > 0, \quad B_1 = (1 + \frac{1}{\tau})[1 + \frac{1}{\tau} + \frac{2p(1+\beta)}{(1+c\beta)^2}] > 0,$$

$$C_1 = -\frac{pc\beta^2 + 2p\beta + p}{\tau(1+c\beta)^2} + [1 + \frac{1}{\tau} + \frac{p(1+\beta)}{(1+c\beta)^2}][\frac{1}{\tau} + (\frac{1}{\tau} + 1)\frac{p(1+\beta)}{(1+c\beta)^2}],$$

$$X_{1,\pm} = \frac{-B_1 \pm \sqrt{B_1^2 - 4A_1C_1}}{2A_1}.$$

When $X_1 \in (-\infty, X_{1,-}) \cup (X_{1,+}, +\infty)$, we can calculate $P_1(0)P_2(0) - P_3(0) > 0$.

Hence, the two conditions in Table 3-1 are satisfied simultaneously, so (s_*, v_*, n_*) is asymptotically stable to (3.3).

3.3. Stability and Turing bifurcation analysis of the diffusive system with nonlocal delay

In this subsection, we study (2.3) as spatial diffusion increases. We analyze the characteristic equation and obtain the conditions of Turing bifurcation generation using the Routh-Hurwitz criterion.

It can be seen from the above analysis that the equilibrium (s_*, v_*, n_*) is locally asymptotically stable when the vegetation-sand system does not consider spatial diffusion. When the vegetation-sand system is coupled with spatial diffusion, it can be concluded from the Routh-Hurwitz criterion that the equilibrium (s_*, v_*, n_*) is stable under the following conditions

$$\begin{cases} P_1(k) > 0, \\ P_3(k) > 0, \\ P_1(k)P_2(k) - P_3(k) > 0. \end{cases}$$

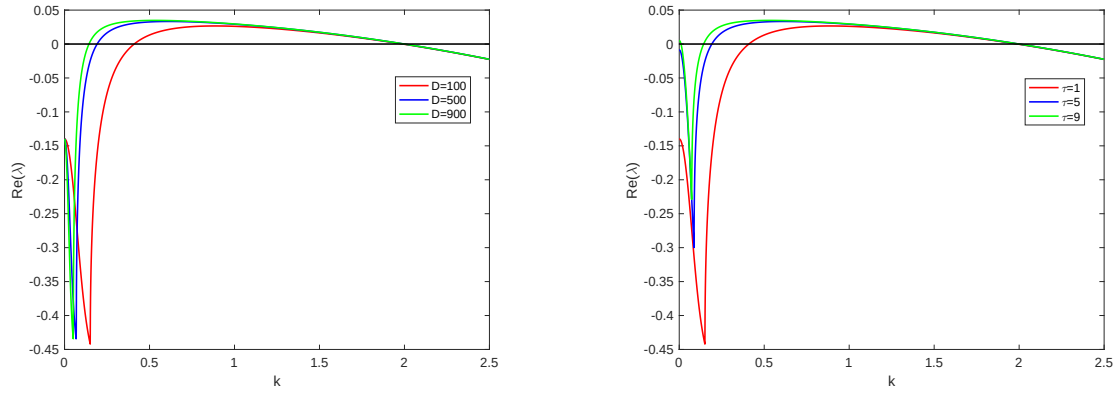

(a) (b)

Figure 1. Impact of D and τ on dispersion of Re(λ) of system (2.3). (a) we plot Re(λ) with respect to different values of D where $\tau = 1$. (b) we plot Re(λ) against different values of τ where $D = 100$. Other parameters are $d = 0.01, h = 1.56, v_m = 400, p = 3.15, c = 3.95$.

Different nonlocal effects correspond with different real part curves of eigenvalues. It is easy to see that in the appropriate parameter range, as the intensity of nonlocal effect gradually increases, the real part of eigenvalue gradually increases and Turing patterns also appear. Obviously, near the equilibrium point (s_*, v_*, n_*), the real part of the eigenvalue of the linearized system (2.3) can be regarded as a function of wave number k. We show the dispersion relation under different nonlocal intensities in Figure 1. The necessary condition for Turing pattern in system (2.3) is that the non-diffusion system is stable, while the diffusion system is unstable. Then, we will analyze the conditions of Turing pattern in equilibrium (s_*, v_*, n_*) from the following three conditions.

Let

$$\begin{pmatrix} s \\ v \\ n \end{pmatrix} = \begin{pmatrix} \varepsilon_1 \\ \varepsilon_2 \\ \varepsilon_3 \end{pmatrix} \exp(\lambda t + ik \cdot \mathbf{r}), \tag{3.4}$$

where k is the wavenumber, λ is the perturbation growth rate in time t, and $i^2 = -1$. The exponential solution (3.4) is substituted into the (2.3) and the following characteristic equation is obtained through calculation

$$\lambda \begin{pmatrix} s \\ v \\ n \end{pmatrix} = \begin{pmatrix} a_{11} - k^2 & a_{12} & a_{13} \\ a_{21} & a_{22} - dk^2 & a_{23} \\ a_{31} & a_{32} & a_{33} - Dk^2 \end{pmatrix} \begin{pmatrix} s \\ v \\ n \end{pmatrix}. \tag{3.5}$$

The solution of the characteristic (3.5) is found and then the dispersion relation is as follows

$$\lambda^3 + P_1(k)\lambda^2 + P_2(k)\lambda + P_3(k) = 0,$$

where

$$P_1(k) = 1 + \frac{1}{\tau} - h + \frac{2h\beta}{v_m} + \frac{p(1+\beta)}{(1+c\beta)^2} + k^2 + dk^2 + Dk^2,$$

$$P_2(k) = [dk^2 - h + \frac{2h\beta}{v_m} + \frac{p(1+\beta)}{(1+c\beta)^2}][Dk^2 + \frac{1}{\tau} + 1 + k^2] + (1+k^2)(Dk^2 + \frac{1}{\tau}),$$

$$P_3(k) = (k^2+1)(dk^2 - h + \frac{2h\beta}{v_m} + \frac{p(1+\beta)}{(1+c\beta)^2})(\frac{1}{\tau} + Dk^2) + \frac{p\beta}{\tau(1+c\beta)}.$$

We show the dispersion relation for different nonlocal effects in Figure 1. A necessary condition for the Turing pattern in (2.3) is that the system is stable in the absence of diffusion and unstable in the presence of diffusion. Therefore, we will analyze the Turing pattern's equilibrium conditions (s_*, v_*, n_*) in the following three conditions.

Condition 1. $P_1(k) > 0$.

Since $k^2 + dk^2 + Dk^2 > 0$ and the equilibrium (s_*, v_*, n_*) is stable without diffusion, Condition 1 always holds.

Condition 2. $P_3(k) > 0$.

Theorem 3.3. *In Condition 2, the equilibrium point of the system is stable in the absence of diffusion and unstable in the presence of diffusion, which is a necessary and sufficient Condition for the Turing pattern. If the inequalities* $f_2^2 - 3f_1f_3 > 0$, $u_{\min} = u_1 > 0$, *and* $F_{\min} = F(u_1) < 0$ *hold, then the Turing bifurcation could occur.*

Proof. Let $P_3(k) = F(k^2)$ and $u = k^2$. Then, $J(k)$ is equivalent to the following expression

$$F(u) = f_3u^3 + f_2u^2 + f_1u + f_0, \tag{3.6}$$

where

$$f_3 = dD > 0, \qquad f_2 = \frac{d}{\tau} + D(-h + \frac{2h\beta}{v_m} + \frac{p(1+\beta)}{(1+c\beta)^2}) + dD,$$

$$f_1 = (\frac{1}{\tau} + D)(-h + \frac{2h\beta}{v_m} + \frac{p(1+\beta)}{(1+c\beta)^2}) + \frac{d}{\tau},$$

$$f_0 = \frac{1}{\tau}(-h + \frac{2h\beta}{v_m} + \frac{p(1+\beta)}{(1+c\beta)^2} + \frac{p\beta}{1+c\beta}).$$

Analyze the properties of the polynomial $F(u)$ as follows.

(i) $\lim\limits_{u\to+\infty} F(u) = +\infty$.

(ii) We can obtain two extremum points by calculating the first partial derivative of (3.2). The forms of the two extreme points are as follows

$$u_1 = \frac{-f_2 + \sqrt{f_2^2 - 3f_1f_3}}{3f_3} \quad \text{and} \quad u_2 = \frac{-f_2 - \sqrt{f_2^2 - 3f_1f_3}}{3f_3}.$$

(iii) We can obtain $F(u)$ second-order deflection by calculating

$$\frac{\mathrm{d}^2F(u)}{\mathrm{d}u^2} = 6f_3u + 2f_2.$$

Using the properties of a unary cubic polynomial, we have

$$u_2 = u_{\max} < u_{\min} = u_1.$$

Thanks to $f_0 > 0$, we obtain that if

$$F_{\min} = F(u_1) < 0$$

is satisfied, Turing bifurcation could occur. Because $u_{\min} = u_1 = \dfrac{-f_2 + \sqrt{f_2^2 - 3f_1f_3}}{3f_3}$ represents the number of the wave, $u_{\min} = u_1 > 0$, to ensure that u_1, u_2 is meaningful, thus $f_2^2 - 3f_1f_3 > 0$.

In Condition 2, if the inequalities $f_2^2 - 3f_1f_3 > 0, u_{\min} = u_1 > 0$, and $F_{\min} = F(u_1) < 0$ hold, then the Turing bifurcation could occur. The proof is completed. Λ

Table 3-2. Analysis methods and necessary and sufficient conditionsfor the formation of Turing pattern.

Methods	Necessary and sufficient condition
	$(f_2)^2 - 3f_1f_3 > 0$
1. Judge the monotonicity of function	$u_{\min} = u_1 > 0$
2. Judge function concavity and convexity	$F(u_{\min}) = F(u_1) < 0$
3. Analyze the necessary and sufficient	$F(0) = P_3(0) > 0$
conditions for Turing pattern	$P_1(0)P_2(0) - P_3(0) > 0$
	$P_1(0) > 0$

Condition 3. $P_1(k)P_2(k) - P_3(k) > 0$.

Theorem 3.4. *If the inequalities* $g_2^2 - 3g_1g_3 > 0, u_{\min} = u_3 > 0$, *and* $G_{\min} = G(u_3) < 0$ *hold, then the Turing bifurcation could occur.*

Proof. Let $G(k^2) = P_1(k)P_2(k) - P_3(k)$ and $u = k^2$. Then, $G(u) = g_3u^3 + g_2u^2 + g_1u + g_0$, where $g_3 = 2dD + d + D + d^2D + d^2 + dD^2 + D^2 > 0$,

$$\begin{aligned} g_2 =&[1 + \frac{1}{\tau} - h + \frac{2h\beta}{v_m} + \frac{p(1+\beta)}{(1+c\beta)^2}][d(D+1) + D] \\ &+ (1 + d + D)[(-h + \frac{2h\beta}{v_m} + \frac{p(1+\beta)}{(1+c\beta)^2})(D+1) + d(\frac{1}{\tau} + 1) + D + \frac{1}{\tau}] - f_2, \\ g_1 =&[1 + \frac{1}{\tau} - h + \frac{2h\beta}{v_m} + \frac{p(1+\beta)}{(1+c\beta)^2}][(D+1)(-h + \frac{2h\beta}{v_m} + \frac{p(1+\beta)}{(1+c\beta)^2}) + d(\frac{1}{\tau} + 1) + D + \frac{1}{\tau}] \\ &+ (1 + d + D)[(\frac{1}{\tau})(-h + \frac{2h\beta}{v_m} + \frac{p(1+\beta)}{(1+c\beta)^2}) + \frac{1}{\tau}] - f_1, \end{aligned}$$

$$g_0 = [1 + \frac{1}{\tau} - h + \frac{2h\beta}{v_m} + \frac{p(1+\beta)}{(1+c\beta)^2}][(-h + \frac{2h\beta}{v_m} + \frac{p(1+\beta)}{(1+c\beta)^2})(\frac{1}{\tau} + 1) + \frac{1}{\tau}] - f_0.$$

Next, analyze the properties of the polynomial $G(u)$

(i) $\lim\limits_{u \to +\infty} G(u) = +\infty$.

(ii) We can obtain two extremum points by calculating the first partial derivative of $G(u)$. The forms of the two extreme points are as follows

$$u_3 = \frac{-g_2 + \sqrt{g_2^2 - 3g_1g_3}}{3g_3} \quad \text{and} \quad u_4 = \frac{-g_2 - \sqrt{g_2^2 - 3g_1g_3}}{3g_3}.$$

(iii) We can obtain $G(u)$ second-order deflection by calculating

$$\frac{\mathrm{d}^2G(u)}{\mathrm{d}u^2} = 6g_3u + 2g_2.$$

Using the properties of a unary cubic polynomial, we get

$$u_4 = u_{\max} < u_{\min} = u_3.$$

Thanks to $g_0 > 0$, we obtain that if the following conditions are satisfied, Turing bifurcation could occur

$$G_{\min} = G(u_3) < 0.$$

Because $u_{\min} = u_3 = \frac{-g_2 + \sqrt{g_2^2 - 3g_1g_3}}{3g_3}$ represents the number of the wave, $u_{\min} = u_3 > 0$, to ensure that u_3, u_4 is meaningful, thus $g_2^2 - 3g_1g_3 > 0$.

Similar to the Condition 2, if the inequalities $g_2^2 - 3g_1g_3 > 0, u_{\min} = u_3 > 0$, and $G_{\min} = G(u_3) < 0$ hold, then the Turing bifurcation could occur. The proof is completed.

Λ

4. Amplitude equation analysis of Turing patterns

In this section, D is the control parameter, and D_T is the bifurcation threshold for the Turing pattern. D is close to the initial D_T, and the eigenvalues are about zero, corresponding to the slow-changing critical mode. In contrast, the off-critical methods relax quickly, so only the perturbation of k around k_T should be considered. We first calculate the critical wave number k_T and bring the necessary k_T into $P_3(k) = 0$ to obtain the bifurcation threshold D_T of the Turing pattern.

According to Theorem 3.3, we get

$$k_T^2 = u_1 = \frac{-f_2 + \sqrt{f_2^2 - 3f_1f_3}}{3f_3}.$$

Therefore, D_T satisfies the following equality

$$\hat{f}_3 k_T^6 + \hat{f}_2 k_T^4 + \hat{f}_1 k_T^2 + \hat{f}_0 = 0,$$

where

$$\hat{f}_3 = dD_T > 0, \qquad \hat{f}_2 = \frac{d}{\tau} + D_T(-h + \frac{2h\beta}{v_m} + \frac{p(1+\beta)}{(1+c\beta)^2}) + dD_T,$$

$$\hat{f}_1 = (\frac{1}{\tau} + D_T)(-h + \frac{2h\beta}{v_m} + \frac{p(1+\beta)}{(1+c\beta)^2}) + \frac{d}{\tau},$$

$$\hat{f}_0 = \frac{1}{\tau}(-h + \frac{2h\beta}{v_m} + \frac{p(1+\beta)}{(1+c\beta)^2} + \frac{p\beta}{1+c\beta}).$$

To obtain the amplitude equation, the perturbation solution $(s - s_*, v - v_*, n - n_*)$ of (2.3) can be represented by $X = (s, v, n)^T$. Then the linearized form of (2.3) near the uniform steady state (s_*, v_*, n_*) is written as follows

$$\begin{cases} \dfrac{\partial s}{\partial t} = a_{11}s + a_{12}v + a_{13}n + W_1(s,v,n) + \nabla^2 s, \\ \dfrac{\partial v}{\partial t} = a_{21}s + a_{22}v + a_{23}n + W_2(s,v,n) + d\nabla^2 v, \\ \dfrac{\partial n}{\partial t} = a_{31}s + a_{32}v + a_{33}n + W_3(s,v,n) + D\nabla^2 n, \end{cases} \tag{4.1}$$

where

$$W_1(s,v,n) = 0, \qquad W_3(s,v,n) = 0,$$

$$W_2(s,v,n) = (-\frac{h}{v_m} + \frac{pcs_*}{(1+cv_*)^3})v^2 - \frac{1}{(1+cv_*)^2}sv - \frac{pc^2s_*}{(1+cv_*)^4}v^3 + \frac{c}{(1+cv_*)^3}sv^2.$$

According to [47], for D sufficiently close to D_T, the solutions of (2.3) can be expanded in a hexagonal planform as

$$X = \begin{pmatrix} s \\ v \\ n \end{pmatrix} = \sum_{j=1}^{3} A_j \exp(i\mathbf{k}_j \cdot \mathbf{r}) + \sum_{j=1}^{3} \overline{A}_j \exp(-i\mathbf{k}_j \cdot \mathbf{r}),$$

in which A_j and $\overline{A}_j$ are the amplitudes corresponding to the modes of $\mathbf{k}_j$ and $-\mathbf{k}_j$. Here $\mathbf{k}_j$ is the wave vector with $|\mathbf{k}_j| = k_T$. Let $W = (W_1, W_2, W_3)^T$. System (4.1) can be expressed as follows

$$\frac{\partial X}{\partial t} = LX + W, \tag{4.2}$$

where

$$L = \begin{pmatrix} a_{11} + \nabla^2 & a_{12} & a_{13} \\ a_{21} & a_{22} + d\nabla^2 & a_{23} \\ a_{31} & a_{32} & a_{33} + D\nabla^2 \end{pmatrix}, \tag{4.3}$$

$$W = \begin{pmatrix} 0 \\ [-\frac{h}{v_m} + \frac{pcs_*}{(1+cv_*)^3}]v^2 - \frac{1}{(1+cv_*)^2}sv - \frac{pc^2s_*}{(1+cv_*)^4}v^3 + \frac{c}{(1+cv_*)^3}sv^2 \\ 0 \end{pmatrix}. \tag{4.4}$$

Since we calculate a sufficiently small neighborhood of the critical value of D, we extend the bifurcation parameter D at D_T

$$D - D_T = \epsilon D_1 + \epsilon^2 D_2 + \epsilon^3 D_3 + O(\epsilon^4), \ \ \epsilon \ll 1. \tag{4.5}$$

By expanding X and the non-linear terms W by the small parameter ϵ, we can obtain

$$X = \begin{pmatrix} s \\ v \\ n \end{pmatrix} = \epsilon \begin{pmatrix} s_1 \\ v_1 \\ n_1 \end{pmatrix} + \epsilon^2 \begin{pmatrix} s_2 \\ v_2 \\ n_2 \end{pmatrix} + \epsilon^3 \begin{pmatrix} s_3 \\ v_3 \\ n_3 \end{pmatrix} + O(\epsilon^4) \tag{4.6}$$

and

$$W = \epsilon^2 Q_2 + \epsilon^3 Q_3 + O(\epsilon^4), \tag{4.7}$$

with

$$Q_2 = \begin{pmatrix} 0 \\ [-\frac{h}{v_m} + \frac{pcs_*}{(1+cv_*)^3}]v_1^2 - \frac{1}{(1+cv_*)^2}s_1v_1] \\ 0 \end{pmatrix},$$

$$Q_3 = \begin{pmatrix} 0 \\ 2[-\frac{h}{v_m} + \frac{pcs_*}{(1+cv_*)^3}]v_1v_2 - \frac{1}{(1+cv_*)^2}[s_1v_2 + s_2v_1] - \frac{pc^2s_*}{(1+cv_*)^4}v_1^3 + \frac{c}{(1+cv_*)^3}s_1v_1^2 \\ 0 \end{pmatrix}.$$

The linear operator L can be decomposed as

$$L = L_T + (D - D_T)N, \tag{4.8}$$

where

$$L_T = \begin{pmatrix} a_{11} + \nabla^2 & a_{12} & a_{13} \\ a_{21} & a_{22} + d\nabla^2 & a_{23} \\ a_{31} & a_{32} & a_{33} + D_T\nabla^2 \end{pmatrix},$$

$$N = \begin{pmatrix} 0 & 0 & 0 \\ 0 & 0 & 0 \\ 0 & 0 & \nabla^2 \end{pmatrix} \triangleq \begin{pmatrix} n_{11} & n_{12} & n_{13} \\ n_{21} & n_{22} & n_{23} \\ n_{31} & n_{32} & n_{33} \end{pmatrix}.$$

Separating the time scale into T_1 and T_2 by the small ϵ through the chain rule of differentiation, we have

$$\frac{\partial}{\partial t} = \frac{\partial}{\partial T_0} + \epsilon \frac{\partial}{\partial T_1} + \epsilon^2 \frac{\partial}{\partial T_2} + O(\epsilon^3), \tag{4.9}$$

with

$$T_0 = t, \quad T_1 = \epsilon t, \quad T_2 = \epsilon^2 t. \tag{4.10}$$

Since the amplitude A_j changes slowly, derivative T_0 does not affect on amplitude A_j. We consider each time scale T_i as an independent variable, and then the reciprocal of time can be obtained as follows

$$\frac{\partial A}{\partial t} = \epsilon \frac{\partial A}{\partial T_1} + \epsilon^2 \frac{\partial A}{\partial T_2} + O(\epsilon^3). \tag{4.11}$$

Substituting (4.3)–(4.11) into (4.2), we have

ϵ :

$$L_T \begin{pmatrix} s_1 \\ v_1 \\ n_1 \end{pmatrix} = 0, \tag{4.12}$$

ϵ^2 :

$$L_T \begin{pmatrix} s_2 \\ v_2 \\ n_2 \end{pmatrix} = \frac{\partial}{\partial T_1} \begin{pmatrix} s_1 \\ v_1 \\ n_1 \end{pmatrix} - D_1 N \begin{pmatrix} s_1 \\ v_1 \\ n_1 \end{pmatrix} - Q_2, \tag{4.13}$$

ϵ^3 :

$$L_T \begin{pmatrix} s_3 \\ v_3 \\ n_3 \end{pmatrix} = \frac{\partial}{\partial T_1} \begin{pmatrix} s_2 \\ v_2 \\ n_2 \end{pmatrix} + \frac{\partial}{\partial T_2} \begin{pmatrix} s_1 \\ v_1 \\ n_1 \end{pmatrix} - D_1 N \begin{pmatrix} s_2 \\ v_2 \\ n_2 \end{pmatrix} - D_2 N \begin{pmatrix} s_1 \\ v_1 \\ n_1 \end{pmatrix} - Q_3. \tag{4.14}$$

As the linear operator of a vegetation-sand system at a critical point, $(s_1, v_1, n_1)^T$ corresponds to the linear combination of the eigenvectors in which the eigenvalue is 0. By calculating (4.12), we can write the corresponding modes of the three wave vectors separately. We have

$$\begin{pmatrix} s_1 \\ v_1 \\ n_1 \end{pmatrix} = \begin{pmatrix} l_1 \\ l_2 \\ 1 \end{pmatrix} (V_1 \exp(i\mathbf{k}_1 \cdot \mathbf{r}) + V_2 \exp(i\mathbf{k}_2 \cdot \mathbf{r}) + V_3 \exp(i\mathbf{k}_3 \cdot \mathbf{r})) + c.c., \tag{4.15}$$

where

$$l_1 = \frac{a_{12}(D_T k_T^2 - a_{33})}{a_{32}(k_T^2 - a_{11})}, \quad l_2 = \frac{D_T k_T^2 - a_{33}}{a_{32}}, \tag{4.16}$$

and $c.c.$ represents the complex conjugate. $V_j(j = 1, 2, 3)$ is the amplitude of $\exp(i\mathbf{k}_j \cdot \mathbf{r})$ which is under first-order perturbation. The perturbation higher-order term determines it.

For (4.13), we get that

$$\begin{aligned} L_T \begin{pmatrix} s_2 \\ v_2 \\ n_2 \end{pmatrix} &= \frac{\partial}{\partial T_1} \begin{pmatrix} s_1 \\ v_1 \\ n_1 \end{pmatrix} - D_1 N \begin{pmatrix} s_1 \\ v_1 \\ n_1 \end{pmatrix} - \begin{pmatrix} 0 \\ [-\frac{h}{v_m} + \frac{pcs_*}{(1+cv_*)^3}]v_1^2 - \frac{1}{(1+cv_*)^2} s_1 v_1] \\ 0 \end{pmatrix} \\ &= \begin{pmatrix} G_s \\ G_v \\ G_n \end{pmatrix}. \end{aligned} \tag{4.17}$$

According to the Fredholm solvability condition, the vector function of the right-hand side of (4.17) must be orthogonal with the zero eigenvectors of the operator L_T^+ to ensure the existence of the non-trivial solution of the (4.17), where L_T^+ is the adjoint operator of L_T. The zero eigenvector of operator L_T^+ is determined by

$$\begin{pmatrix} 1 \\ l_2^+ \\ l_3^+ \end{pmatrix} \exp(-i\mathbf{k}_j \cdot \mathbf{r}), j = 1, 2, 3,$$

where

$$l_2^+ = \frac{k_T^2 - a_{11}}{a_{21} + dk_T^2}, \quad l_3^+ = \frac{a_{23}(k_T^2 - a_{11})}{(D_T k_T^2 - a_{33})(a_{21} + dk_T^2)}. \tag{4.18}$$

Customarily, $G_s^j, G_v^j, G_n^j (j = 1, 2, 3)$ are the coefficients corresponding to $\exp(i\mathbf{k}_j \cdot \mathbf{r})$ in G_s, G_v and G_n respectively. Therefore, substituting (4.15) into (4.17) and sorting out the coefficients of $\exp(i\mathbf{k}_1 \cdot \mathbf{r})$, $\exp(i\mathbf{k}_2 \cdot \mathbf{r})$, and $\exp(i\mathbf{k}_3 \cdot \mathbf{r})$. Using the Fredholm solvability condition, we obtain the following system

$$\begin{pmatrix} G_s^1 \\ G_v^1 \\ G_n^1 \end{pmatrix} = \begin{pmatrix} l_1 \\ l_2 \\ 1 \end{pmatrix} \frac{\partial V_1}{\partial T_1} - D_1 N \begin{pmatrix} l_1 \\ l_2 \\ 1 \end{pmatrix} V_1 - \begin{pmatrix} G_1 \\ F_1 \\ E_1 \end{pmatrix} \overline{V}_2 \overline{V}_3,$$

$$\begin{pmatrix} G_s^2 \\ G_v^2 \\ G_n^2 \end{pmatrix} = \begin{pmatrix} l_1 \\ l_2 \\ 1 \end{pmatrix} \frac{\partial V_2}{\partial T_1} - D_1 N \begin{pmatrix} l_1 \\ l_2 \\ 1 \end{pmatrix} V_2 - \begin{pmatrix} G_1 \\ F_1 \\ E_1 \end{pmatrix} \overline{V}_1 \overline{V}_3,$$

$$\begin{pmatrix} G_s^3 \\ G_v^3 \\ G_n^3 \end{pmatrix} = \begin{pmatrix} l_1 \\ l_2 \\ 1 \end{pmatrix} \frac{\partial V_3}{\partial T_1} - D_1 N \begin{pmatrix} l_1 \\ l_2 \\ 1 \end{pmatrix} V_3 - \begin{pmatrix} G_1 \\ F_1 \\ E_1 \end{pmatrix} \overline{V}_1 \overline{V}_2,$$

where

$$\begin{pmatrix} G_1 \\ F_1 \\ E_1 \end{pmatrix} = 2\begin{pmatrix} 0 \\ [-\frac{h}{v_m} + \frac{pcs_*}{(1+cv_*)^3}]l_2^2 - \frac{1}{1+cv_*}l_1 l_2 \\ 0 \end{pmatrix}. \tag{4.19}$$

Applying orthogonal condition

$$(1, l_2^+, l_3^+)\begin{pmatrix} G_s^j \\ G_v^j \\ G_n^j \end{pmatrix} = 0, \quad j = 1, 2, 3,$$

we can obtain that

$$\begin{cases} (l_1 + l_2 l_2^+ + l_3^+)\dfrac{\partial V_1}{\partial T_1} = D_1 H V_1 + (G_1 + l_2^+ F_1)\overline{V}_2\overline{V}_3, \\ (l_1 + l_2 l_2^+ + l_3^+)\dfrac{\partial V_2}{\partial T_1} = D_1 H V_2 + (G_1 + l_2^+ F_1)\overline{V}_1\overline{V}_3, \\ (l_1 + l_2 l_2^+ + l_3^+)\dfrac{\partial V_3}{\partial T_1} = D_1 H V_3 + (G_1 + l_2^+ F_1)\overline{V}_1\overline{V}_2, \end{cases} \tag{4.20}$$

where

$$H = (1, l_2^+, l_3^+)N\begin{pmatrix} l_1 \\ l_2 \\ 1 \end{pmatrix} = -k_T^2 l_3^+. \tag{4.21}$$

The system of (4.20) is an amplitude equation with first-order perturbation. We can find that the second-order coefficient of the equation is more significant than zero. Then, we can get amplitude $V_j (j = 1, 2, 3)$ diverges. So, introducing higher-order perturbation terms into the solution of (4.13) is necessary, such as $\exp(2i\mathbf{k}_j \cdot \mathbf{r})$, $\exp(i(\mathbf{k}_1 - \mathbf{k}_2) \cdot \mathbf{r})$, and so on.

$$\begin{aligned} \begin{pmatrix} s_2 \\ v_2 \\ n_2 \end{pmatrix} = \begin{pmatrix} S_0 \\ V_0 \\ N_0 \end{pmatrix} + \sum_{j=1}^{3}\begin{pmatrix} S_j \\ V_j \\ N_j \end{pmatrix}\exp(i\mathbf{k}_j \cdot \mathbf{r}) + \sum_{j=1}^{3}\begin{pmatrix} S_{jj} \\ V_{jj} \\ N_{jj} \end{pmatrix}\exp(2i\mathbf{k}_j \cdot \mathbf{r}) \\ + \begin{pmatrix} S_{12} \\ V_{12} \\ N_{12} \end{pmatrix}\exp(i(\mathbf{k}_1 - \mathbf{k}_2) \cdot \mathbf{r}) + \begin{pmatrix} S_{23} \\ V_{23} \\ N_{23} \end{pmatrix}\exp(i(\mathbf{k}_2 - \mathbf{k}_3) \cdot \mathbf{r}) \\ + \begin{pmatrix} S_{31} \\ V_{31} \\ N_{31} \end{pmatrix}\exp(i(\mathbf{k}_3 - \mathbf{k}_1) \cdot \mathbf{r}) + c.c., \end{aligned} \tag{4.22}$$

with

$$\begin{pmatrix} S_0 \\ V_0 \\ N_0 \end{pmatrix} = \begin{pmatrix} Y_{S_0} \\ Y_{V_0} \\ Y_{N_0} \end{pmatrix} (|V_1|^2 + |V_2|^2 + |V_3|^2), \quad V_j = l_2 N_j, \qquad S_j = l_1 N_j,$$

$$\begin{pmatrix} S_{jj} \\ V_{jj} \\ N_{jj} \end{pmatrix} = \begin{pmatrix} Y_{S_1} \\ Y_{V_1} \\ Y_{N_1} \end{pmatrix} V_j^2, \quad \begin{pmatrix} S_{12} \\ V_{12} \\ N_{12} \end{pmatrix} = \begin{pmatrix} Y_{S_2} \\ Y_{V_2} \\ Y_{N_2} \end{pmatrix} V_1 \overline{V}_2,$$

$$\begin{pmatrix} S_{23} \\ V_{23} \\ N_{23} \end{pmatrix} = \begin{pmatrix} Y_{S_2} \\ Y_{V_2} \\ Y_{N_2} \end{pmatrix} V_2 \overline{V}_3, \quad \begin{pmatrix} S_{31} \\ V_{31} \\ N_{31} \end{pmatrix} = \begin{pmatrix} Y_{S_2} \\ Y_{V_2} \\ Y_{N_2} \end{pmatrix} V_3 \overline{V}_1,$$

where

$$\begin{pmatrix} Y_{S_0} \\ Y_{V_0} \\ Y_{N_0} \end{pmatrix} = - \begin{pmatrix} a_{11} & a_{12} & a_{13} \\ a_{21} & a_{22} & a_{23} \\ a_{31} & a_{32} & a_{33} \end{pmatrix}^{-1} \begin{pmatrix} G_1 \\ F_1 \\ E_1 \end{pmatrix},$$

$$\begin{pmatrix} Y_{S_1} \\ Y_{V_1} \\ Y_{N_1} \end{pmatrix} = -\frac{1}{2} \begin{pmatrix} a_{11} - 4k_T^2 & a_{12} & a_{13} \\ a_{21} & a_{22} - 4dk_T^2 & a_{23} \\ a_{31} & a_{32} & a_{33} - 4D_T k_T^2 \end{pmatrix}^{-1} \begin{pmatrix} G_1 \\ F_1 \\ E_1 \end{pmatrix},$$

$$\begin{pmatrix} Y_{S_2} \\ Y_{V_2} \\ Y_{N_2} \end{pmatrix} = - \begin{pmatrix} a_{11} - 3k_T^2 & a_{12} & a_{13} \\ a_{21} & a_{22} - 3dk_T^2 & a_{23} \\ a_{31} & a_{32} & a_{33} - 3D_T k_T^2 \end{pmatrix}^{-1} \begin{pmatrix} G_1 \\ F_1 \\ E_1 \end{pmatrix}.$$

For (4.14), we get that

$$\begin{aligned} L_T \begin{pmatrix} s_3 \\ v_3 \\ n_3 \end{pmatrix} &= \frac{\partial}{\partial T_1} \begin{pmatrix} s_2 \\ v_2 \\ n_2 \end{pmatrix} + \frac{\partial}{\partial T_2} \begin{pmatrix} s_1 \\ v_1 \\ n_1 \end{pmatrix} - D_1 N \begin{pmatrix} s_2 \\ v_2 \\ n_2 \end{pmatrix} - D_2 N \begin{pmatrix} s_1 \\ v_1 \\ n_1 \end{pmatrix} - Q_3 \\ &= \frac{\partial}{\partial T_1} \begin{pmatrix} s_2 \\ v_2 \\ n_2 \end{pmatrix} + \frac{\partial}{\partial T_2} \begin{pmatrix} s_1 \\ v_1 \\ n_1 \end{pmatrix} - D_1 N \begin{pmatrix} s_2 \\ v_2 \\ n_2 \end{pmatrix} - D_2 N \begin{pmatrix} s_1 \\ v_1 \\ n_1 \end{pmatrix} \\ &- \begin{pmatrix} 0 \\ 2[-\frac{h}{v_m} + \frac{pcs_*}{(1+cv_*)^3}]v_1 v_2 - \frac{1}{(1+cv_*)^2}[s_1 v_2 + s_2 v_1] - \frac{pc^2 s_*}{(1+cv_*)^4} v_1^3 + \frac{c}{(1+cv_*)^3} s_1 v_1^2 \\ 0 \end{pmatrix} \\ &= \begin{pmatrix} F_s \\ F_v \\ F_n \end{pmatrix}. \end{aligned}$$

Substituting the solutions (4.15) and (4.22) of the upper two order perturbation equation into (4.14) and sorting out the coefficients of $\exp(i\mathbf{k}_1 \cdot \mathbf{r})$, and $\exp(i\mathbf{k}_2 \cdot \mathbf{r})$, and $\exp(i\mathbf{k}_3 \cdot \mathbf{r})$ by using the Fredholm solvability condition, we obtain the following system

$$\begin{aligned}\begin{pmatrix} F_s^1 \\ F_v^1 \\ F_n^1 \end{pmatrix} &= \begin{pmatrix} l_1 \\ l_2 \\ 1 \end{pmatrix}\left(\frac{\partial V_1}{\partial T_2} + \frac{\partial N_1}{\partial T_1}\right) - D_1 N \begin{pmatrix} l_1 \\ l_2 \\ 1 \end{pmatrix} N_1 - D_2 N \begin{pmatrix} l_1 \\ l_2 \\ 1 \end{pmatrix} V_1 \\ &\quad - \begin{pmatrix} G_1 \\ F_1 \\ E_1 \end{pmatrix}(\overline{V}_2\overline{N}_3 + \overline{V}_3\overline{N}_2) - \begin{pmatrix} G_2 \\ F_2 \\ E_2 \end{pmatrix}|V_1|^2 V_1 - \begin{pmatrix} G_3 \\ F_3 \\ E_3 \end{pmatrix}(|V_2|^2 + |V_3|^2)V_1,\end{aligned}$$

where

$$\begin{cases} G_2 = 0, \\ F_2 = -\dfrac{p}{(1+cv_*)^2}(l_1 Y_{V_0} + l_2 Y_{S_0}) + \dfrac{2pcs_*}{(1+cv_*)^3} l_2 Y_{V_0} - \dfrac{p}{(1+cv_*)^2}(l_1 Y_{V_1} + l_2 Y_{S_1}) \\ \quad + \dfrac{2pcs_*}{(1+cv_*)^3} l_2 Y_{V_1} + \dfrac{3pc}{(1+cv_*)^3} l_1 l_2^2 - \dfrac{3pc^2 s_*}{(1+cv_*)^4}, \\ E_2 = 0, \end{cases} \tag{4.23}$$

and

$$\begin{cases} G_3 = 0, \\ F_3 = -\dfrac{p}{(1+cv_*)^2}(l_1 Y_{V_0} + l_2 Y_{S_0}) + \dfrac{2pcs_*}{(1+cv_*)^3} l_2 Y_{V_0} - \dfrac{p}{(1+cv_*)^2}(l_1 Y_{V_2} + l_2 Y_{S_2}) \\ \quad + \dfrac{2pcs_*}{(1+cv_*)^3} l_2 Y_{V_2} + \dfrac{6pc}{(1+cv_*)^3} l_1 l_2^2 - \dfrac{6pc^2 s_*}{(1+cv_*)^4}, \\ E_3 = 0. \end{cases} \tag{4.24}$$

Applying orthogonal condition

$$(1, l_2^+, l_3^+)\begin{pmatrix} F_s^j \\ F_v^j \\ F_n^j \end{pmatrix} = 0, \quad j = 1, 2, 3,$$

we can obtain that

$$\begin{aligned}(l_1 + l_2 l_2^+ + l_3^+)\left(\frac{\partial V_1}{\partial T_2} + \frac{\partial N_1}{\partial T_1}\right) &= H(D_1 N_1 + D_2 V_1) + (G_1 + F_1 l_2^+)(\overline{V}_2\overline{N}_3 + \overline{V}_3\overline{N}_2) \\ &\quad + (G_2 + F_2 l_2^+)|V_1|^2 V_1 + (G_3 + F_3 l_2^+)(|V_2|^2 + |V_3|^2)V_1.\end{aligned} \tag{4.25}$$

The amplitude A_j is the coefficient of $\exp(i\mathbf{k}_j \cdot \mathbf{r})(j = 1, 2, 3)$ at each level. We have

$$A_j = \epsilon V_j + \epsilon^2 N_j + O(\epsilon^3).$$

Together with (4.9), (4.10), (4.20), and (4.25), the amplitude equations about A_j are as follows

$$\begin{cases} \tau_0\dfrac{\partial A_1}{\partial t} = \phi A_1 + \eta\overline{A}_2\overline{A}_3 - [Z_1|A_1|^2 + Z_2(|A_2|^2 + |A_3|^2)]A_1, \\ \tau_0\dfrac{\partial A_2}{\partial t} = \phi A_2 + \eta\overline{A}_1\overline{A}_3 - [Z_1|A_2|^2 + Z_2(|A_3|^2 + |A_1|^2)]A_1, \\ \tau_0\dfrac{\partial A_3}{\partial t} = \phi A_3 + \eta\overline{A}_1\overline{A}_2 - [Z_1|A_3|^2 + Z_2(|A_1|^2 + |A_2|^2)]A_1, \end{cases} \tag{4.26}$$

with

$$\tau_0 = \frac{l_1 + l_2 l_2^+ + l_3^+}{D_T H}, \quad \phi = \frac{D - D_T}{D_T}, \quad \eta = \frac{G_1 + F_1 l_2^+}{D_T H},$$

$$Z_1 = -\frac{G_2 + F_2 l_2^+}{D_T H}, \quad Z_2 = -\frac{G_3 + F_3 l_2^+}{D_T H},$$

where $l_1, l_2, l_2^+, l_3^+, G_1, F_1, H, G_2, F_2, G_3$, and F_3 are defined as (4.16), (4.18), (4.19), (4.21), (4.23), and (4.24).

Next, we study the stability of the amplitude equation of the vegetation-sand model. We can construct different types of pattern structures in Turing space, and a stable Turing pattern structure is a steady-state solution for the corresponding (4.26). Each amplitude of (4.26) can be decomposed into a corresponding mode $\gamma_i = |A_i|$ and phase angle θ_i. By substituting $A_i = \gamma_i exp(i\theta_i)$ into (4.26) and separating the real part from the imaginary part, we can get

$$\begin{cases} \tau_0\dfrac{\partial \theta}{\partial t} = -\eta\dfrac{\gamma_1^2\gamma_2^2 + \gamma_2^2\gamma_3^2 + \gamma_3^2\gamma_1^2}{\gamma_1\gamma_2\gamma_3}\sin\theta, \\ \tau_0\dfrac{\partial \gamma_1}{\partial t} = \phi\gamma_1 + \eta\gamma_2\gamma_3\cos\theta - [Z_1|\gamma_1^2 + Z_2(\gamma_2^2 + \gamma_3^2)]\gamma_1, \\ \tau_0\dfrac{\partial \gamma_2}{\partial t} = \phi\gamma_2 + \eta\gamma_1\gamma_3\cos\theta - [Z_1|\gamma_2^2 + Z_2(\gamma_1^2 + \gamma_3^2)]\gamma_2, \\ \tau_0\dfrac{\partial \gamma_3}{\partial t} = \phi\gamma_3 + \eta\gamma_1\gamma_2\cos\theta - [Z_1|\gamma_3^2 + Z_2(\gamma_1^2 + \gamma_2^2)]\gamma_3, \end{cases} \tag{4.27}$$

where $\theta = \theta_1 + \theta_2 + \theta_3$. The following conclusions can be drawn for (4.27).

Theorem 4.1. *For homogeneous reaction-diffusion systems, assume that $Z_1 > 0$ and $Z_2 > 0$.*

*(i) A uniform steady state solution (**O**): $\gamma_1 = \gamma_2 = \gamma_3 = 0$. If $\phi < \phi_2 = 0$, then (**O**) is stable. If $\phi > \phi_2 = 0$, then (**O**) is unstable.*

*(ii) A stripe pattern diagram (**S**): $\gamma_1 = \sqrt{\frac{\phi}{Z_1}} \neq 0$, $\gamma_2 = \gamma_3 = 0$ with $\phi > \phi_2 = 0$. If $\phi > \phi_3 = \frac{\eta^2 Z_1}{(Z_2 - Z_1)^2}$, then (**S**) is stable. If $\phi < \phi_3$, then (**S**) is unstable.*

(iii) Two hexagonal layouts ($\boldsymbol{H_0}, \boldsymbol{H_\pi}$): $\gamma_1 = \gamma_2 = \gamma_3 = \frac{|\eta| \pm \sqrt{\eta^2 + 4(Z_1 + 2Z_2)\phi}}{2(Z_1 + 2Z_2)}$ with $\phi > \phi_1 = -\frac{\eta^2}{4(Z_1 + 2Z_2)^2}$. If $\phi < \phi_4 = \frac{(2Z_1 + Z_2)\eta^2}{(Z_2 - Z_1)}$, then the solution $\gamma^+ = \frac{|\eta| + \sqrt{\eta^2 + 4(Z_1 + 2Z_2)\phi}}{2(Z_1 + 2Z_2)}$ is stable and the other solution $\gamma^- = \frac{|\eta| - \sqrt{\eta^2 + 4(Z_1 + 2Z_2)\phi}}{2(Z_1 + 2Z_2)}$ is unstable.

*(iv) A mixed structure solution (**MS**): $\gamma_1 = \frac{|\eta|}{Z_2 - Z_1}, \gamma_2 = \gamma_3 = \sqrt{\frac{\phi - Z_1\gamma_1^2}{Z_1 + Z_2}}$, which exists under the condition $\phi > \phi_3$ and $Z_2 > Z_1$, and the solution is always unstable.*

Table 1. The values of each parameter in Figure 2.

τ	η	ϕ	ϕ_1	ϕ_2	ϕ_3	ϕ_4	range of ϕ
0.35	101.3345	0.6	-0.6580	0	13.6740	13.6471	$\phi_1 < \phi_2 < \phi < \phi_3 < \phi_4$
0.33	89.4032	0.5	-0.0441	0	0.0027	0.6607	$\phi_1 < \phi_2 < \phi_3 < \phi < \phi_4$
0.31	77.3125	0.5120	-0.0101	0	0.1019	0.2039	$\phi_1 < \phi_2 < \phi_3 < \phi_4 < \phi$

It should be pointed out that when $\tau_0 > 0$, this means that if $\eta > 0$, then the stable hexagon pattern is $H_0(\theta = 0)$ and $H_\pi(\theta = \pi)$ is unstable; if $\eta < 0$, then the stable hexagon pattern is $H_\pi(\theta = \pi)$ and $H_0(\theta = 0)$ is unstable.

Theorem 4.2. *In the interval where Turing pattern is generated, other parameters are fixed and D and τ are set as variable parameters.*

(i) When $\phi_2 < \phi < \phi_3$, the system (2.3) appears spot pattern.

(ii) When $\phi_3 < \phi < \phi_4$, according to different initial conditions, the system (2.3) appears spot pattern or stripe pattern.

(iii) When $\phi > \phi_4$, the spot pattern in the system (2.3) is transformed to the stripe pattern.

5. Numerical simulations

In this section, we give some numerical simulations to support the theoretical results obtained in the above section. Choose a region of size 30×30 whose boundary satisfies Neumann boundary conditions. We set the time region as [0, 96] and the time step as $\Delta t = 0.002$. The initial value is the random perturbation at the equilibrium point (s_*, v_*, n_*). The simulation program runs until the main features of the pattern do not seem to change.

(1) We use numerical simulation to verify the above theoretical analysis. Selecting the values of different parameters h, p, v_m, c, d, and D, we can calculate the values of η, Z_1, Z_2, ϕ_1, ϕ_2, ϕ_3, ϕ_4, and ϕ according to the expression of the amplitude equation coefficients in Section 4. In order to observe the pattern structure of vegetation, we fix the other parameters and select three sets of parameters that differ only in the value of τ. We continue to keep $d = 0.01, h = 2.8, vm = 4, p = 3.9, c = 3$, and $D = 3$. When $\tau = 0.35$, the spot pattern appears in Figure 2(a); As τ decreases, the vegetation pattern structure shows mixed pattern of stripe and spot pattern (see Figure 2(b)); Figure 2(c) transforms into stripe pattern when $\tau = 0.31$. Choose a region of size 90×90 whose boundary satisfies Neumann boundary conditions. The corresponding results are shown in Fig 2. Specifically, when the first set of parameter values is taken, ϕ is between ϕ_2 and ϕ_3, and system (1.3) presents a spot pattern (see Figure 2(a)); when the second set of parameter values is taken, ϕ is between ϕ_3 and ϕ_4, the spot pattern loses its stability and the stripe pattern begins to appear, showing a mixed pattern (see Figure 2(b)); when the third set of parameter values is taken, ϕ is greater than ϕ_4, and the spot pattern disappears to a striped pattern (see Figure 2(c)). All our simulations are carried out on the basis of Table 1 at τ.

(2) Let $h = 24.56, p = 17, v_m = 10, c = 0.2, \tau = 10$. The equilibrium (s_*, v_*, n_*) is locally asymptotically stable for (3.3). See Figure 3. Let $h = 26, p = 17, v_m = 10, c = 0.2, \tau = 10$. The equilibrium (s_*, v_*, n_*) is unstable for (3.3). See Figure 4. Choose the initial conditions $(s_0, v_0, n_0) = (2.1, 2.6, 2.1)$.

(3) Let $h = 3.3333, p = 2.8245, v_m = 10, c = 3.1111, d = 100$, and $(s_0, v_0) = (8.0248 + 1.337\cos 3x, 7.0248 + 1.337\cos 3x)$. The conditions $0 < H < 1, H < N$, and $d > z_1$ hold true. By

Theory 3.1, the equilibrium (s_*, v_*) is stable for system (3.1). See Figure 5. Take $h = 3.3333, p = 2.1234, v_m = 10, c = 1.1111, d = 0.00061$, and $(s_0, v_0) = (5.1533 + 1.337\cos 1.7x, 4.1533 + 1.337\cos 1.7x)$. Then, $d \to 0^+$ hold. Hence, by Theory 3.2, the equilibrium (s_*, v_*) is Turing unstable for system (3.1). See Figure 6. Let $h = 3.3333, p = 2.8245, v_m = 10, c = 1.1111, d = 1$, and $(s_0, v_0) = (3.1213 + 1.337\cos 1.7x, 2.1213 + 1.337\cos 1.7x)$. System (3.1) can induce spatially inhomogeneous Hopf bifuracation. See Figure 7.

(4) Let $d = 0.01, h = 2.8, v_m = 4, p = 3.9, c = 3, D = 1$. Figure 8 shows the succession of vegetation pattern when $\tau = 0.01$. It can be seen from the figure, as time goes on, the vegetation patterns evolves from an initially uniform distribution to gradually uneven clustering, forming gapped patterns, and eventually reaching stability where it no longer changes with time.

(5) Let $d = 0.01, h = 2.8, v_m = 4, p = 3.9, c = 3, D = 1$. Figure 9 shows the vegetation pattern in the final stable state with different delays. As τ gradually increases, we observed that the vegetation patterns formed gapped, clustered, and ring-like patterns, with vegetation transitioning from dense to gradually sparse. This reflects the nonlocal delayed impact of aeolian sand on vegetation. The greater the delay, the higher the degree of vegetation destruction, resulting in a sparser distribution.

(6) In Figure 10, we consider the effect of the destruction by sand burial p on vegetation pattern structure. Let $d = 0.01, h = 2.8, v_m = 4, c = 3, D = 1, \tau = 0.01$. When the parameter p is small, the gap pattern appears (Figure 10(a)); as the parameter p continues to increase, the spot pattern appears, showing the spot stripe mixed pattern (Figure 10(c)); when the parameter p further increases, the vegetation patches form a ring-like pattern.

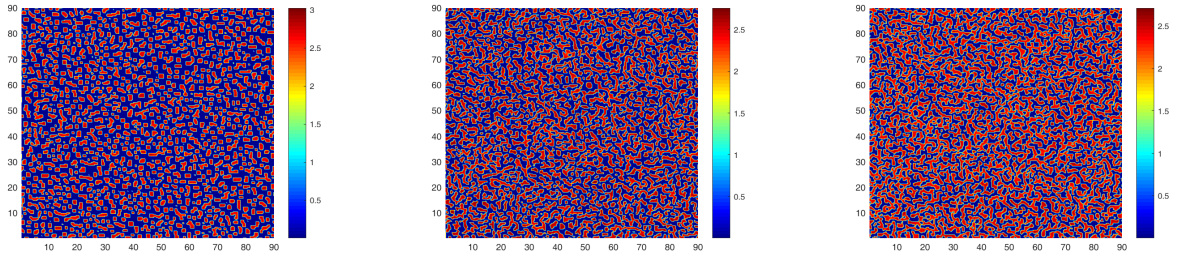

(a) (b) (c)

Figure 2. The pattern structure corresponding to different values of parameter τ. Parameter values: $d = 0.01, h = 2.8, v_m = 4, p = 3.9, c = 3, D = 3$.

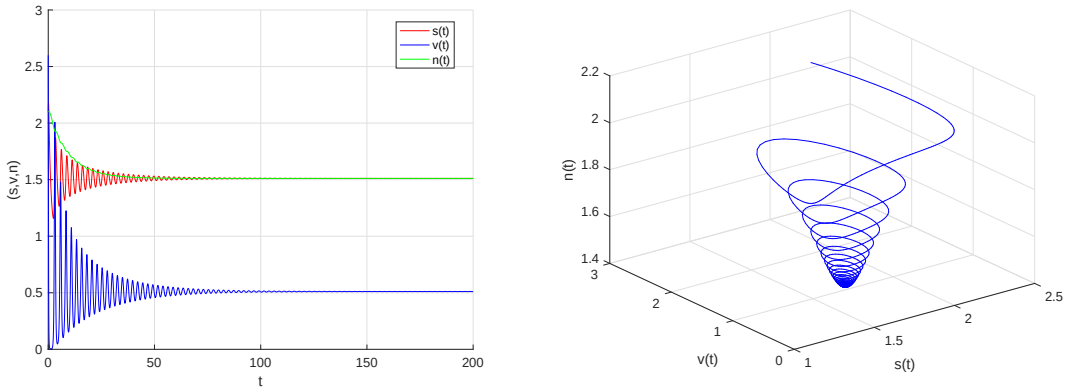

(a) Time diagram (b) Phase diagram

Figure 3. The equilibrium (s_*, v_*, n_*) of system (3.3) is locally asymptotically stable for $h = 24.56, p = 17, v_m = 10, c = 0.2, \tau = 10$.

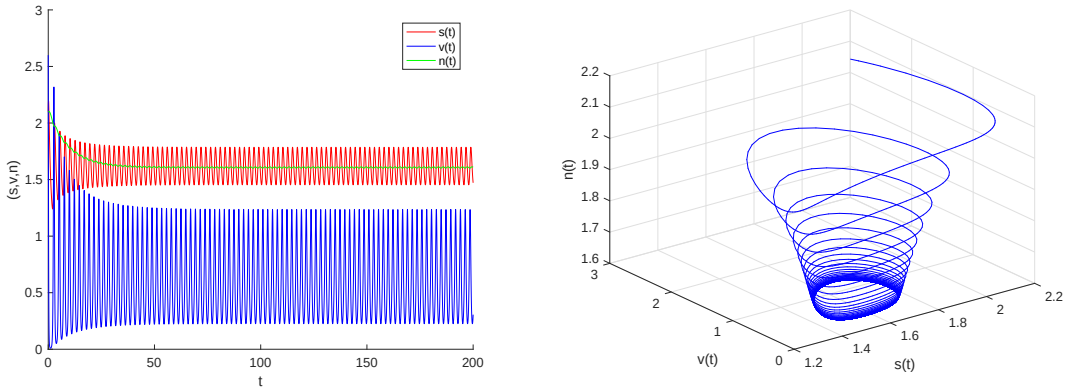

(a) Time diagram (b) Phase diagram

Figure 4. The equilibrium (s_*, v_*, n_*) of system (3.3) is unstable for $h = 26, p = 17$, $v_m = 10, c = 0.2, \tau = 10$.

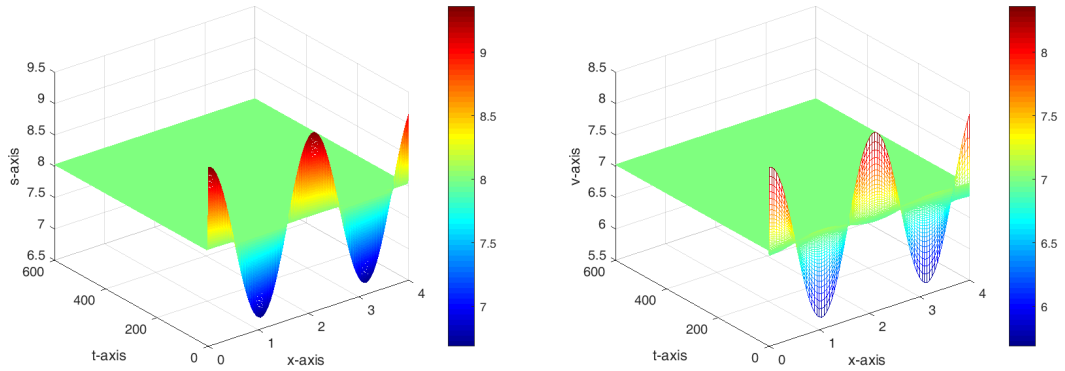

Figure 5. The equilibrium (s_*, v_*) of system (3.1) is stable for $h = 3.3333, p = 2.8245$, $v_m = 10, c = 3.1111, d = 100$.

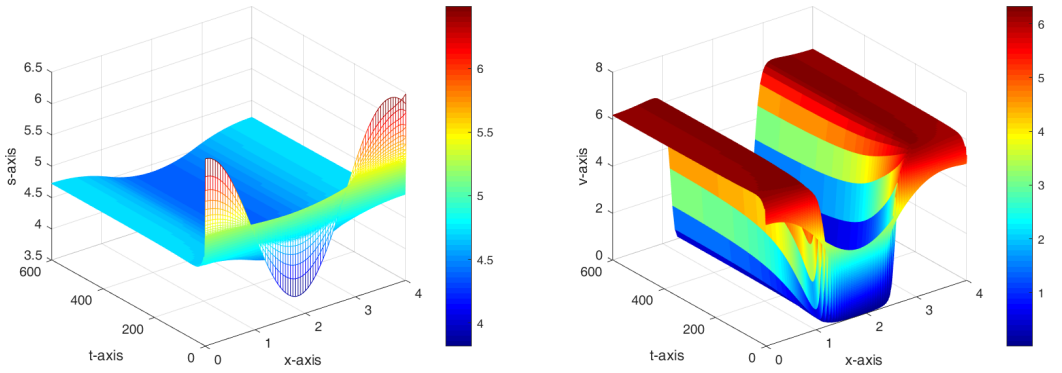

Figure 6. The equilibrium (s_*, v_*) of system (3.1) is Turing unstable for $h = 3.3333$, $p = 2.1234, v_m = 10, c = 1.1111, d = 0.00061$.

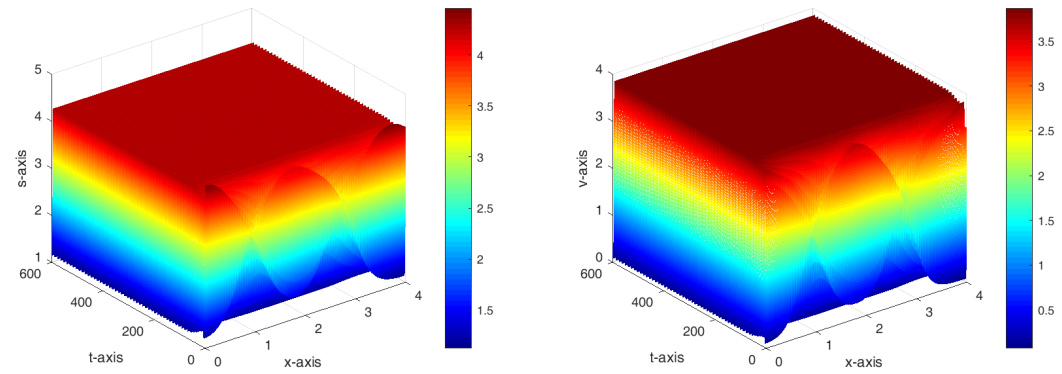

Figure 7. Positive periodic solution of (3.1) for $h = 3.3333$, $p = 2.8245$, $v_m = 10$, $c = 1.1111, d = 1$.

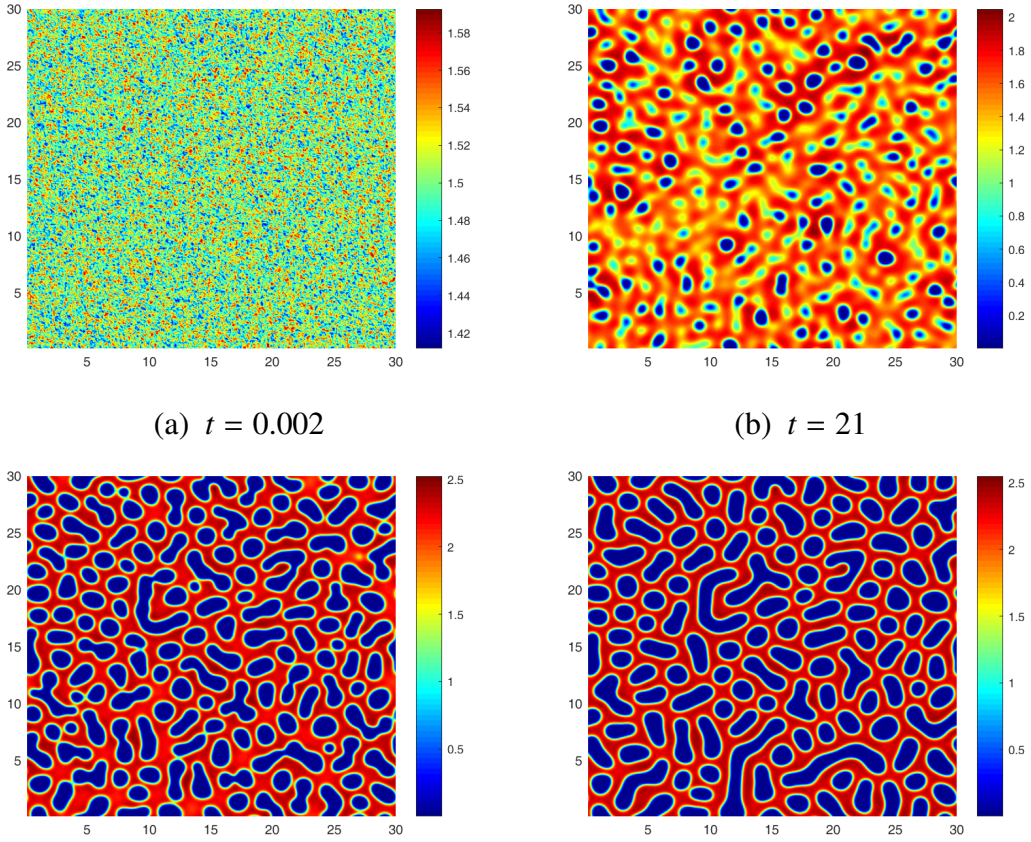

(a) $t = 0.002$ (b) $t = 21$

(c) $t = 36$ (d) $t = 96$

Figure 8. Patterned plant distribution in system (2.3) with $d = 0.01, h = 2.8, v_m = 4$, $p = 3.9, c = 3, D = 1$. Here, $\tau = 0.01$. (a) $t = 0.002$; (b) $t = 21$; (c) $t = 36$; (d) $t = 96$.

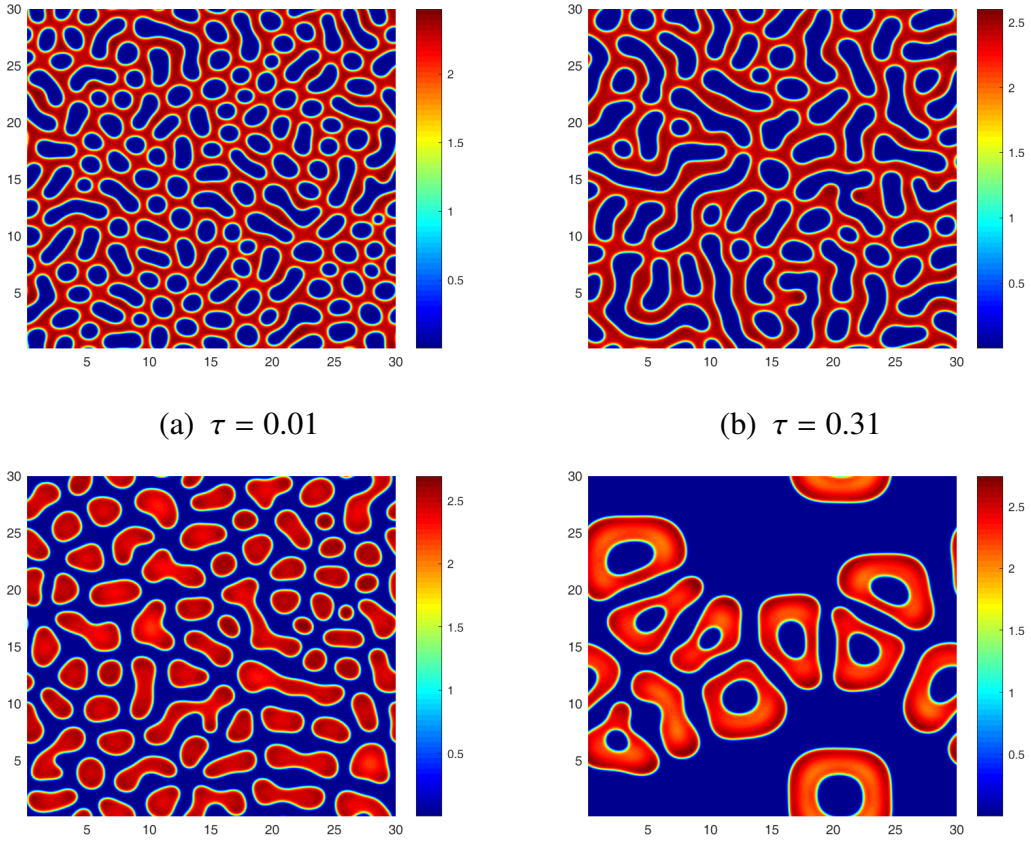

(a) $\tau = 0.01$ (b) $\tau = 0.31$

(c) $\tau = 0.34$ (d) $\tau = 0.35$

Figure 9. When $d = 0.01, h = 2.8, v_m = 4, p = 3.9, c = 3, D = 1$, different τ corresponds to the vegetation patterns. (a) $\tau = 0.01$; (b) $\tau = 0.31$; (c) $\tau = 0.34$; (d) $\tau = 0.35$.

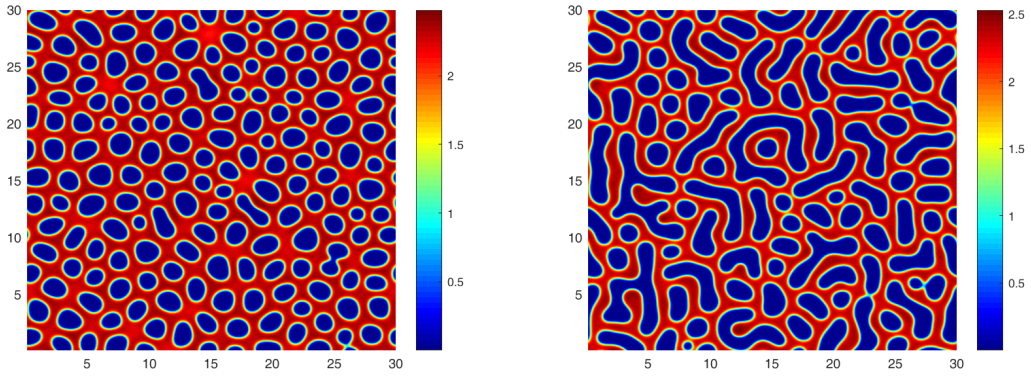

(a) $p = 3.75$ (b) $p = 4.01$

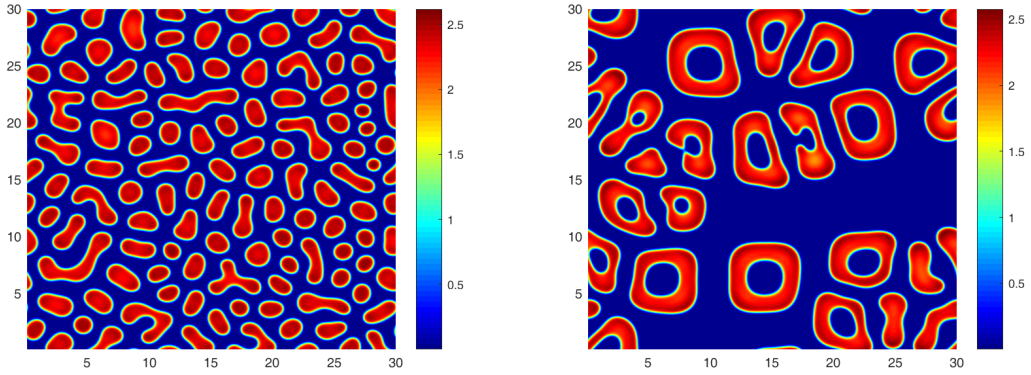

(c) $p = 4.15$ (d) $p = 4.17$

Figure 10. Effects of the destruction by sand burial p on vegetation pattern structure. (a) $p = 3.75$; (b) $p = 4.01$; (c) $p = 4.15$; (d) $p = 4.17$. The other parameter values are $d = 0.01, h = 2.8, v_m = 4, c = 3, D = 1, \tau = 0.01$.

6. Conclusions

Aeolian sand vegetation patterns have been observed and described for a long time, but there are few explorations on their formation mechanisms. To explore the ecological mechanism of its formation, to enrich the scenarios of vegetation competition for resources in different ecosystems, and to deepen the understanding of desertification and vegetation restoration process, this paper mainly investigates the spatial and temporal complexity of vegetation in arid and semi-arid regions from the aspects of vegetation system modelling and theoretical analysis. First, a vegetation model with nonlocal effects is constructed, the equilibrium state of the model is calculated, linear analysis is carried out at the equilibrium state, and the spatio-temporal dynamics of the model are investigated. Second, the theoretical basis of vegetation for combating desertification is proposed. Finally, the effect of the nonlocal delay on the vegetation sand model is shown through numerical simulation.

The effect of nonlocal delay on vegetation patterns is as follows: a certain range as τ increases, the density of vegetation decreases, which reflects that the ability of sand to destroy vegetation increases as τ increases, so the nonlocal delay can change the structure of vegetation pattern. In terms of theoretical analysis, Turing space was obtained using linearized analysis for the model, but the pattern structure and its stability could not be determined. Amplitude equations that can describe the dynamical behaviour of the system near the destabilisation point of the vegetation model were derived using nonlinear analysis, both to describe the different parameter spaces corresponding to different patterns and to determine whether the corresponding patterns are stable or not, which makes up for the shortcomings of the linear analysis method.

The improved vegetation-sand dynamics model in this paper is theoretical. The theoretical model is widely accepted in the field of vegetation pattern, which explains the main mechanism of the vegetation pattern formation process and promotes the research process of nonlocal delay of the vegetation-sand model, but it is still difficult to explore the more complex vegetation-sand model, such as the addition of the advection term and so on, to a certain extent. For studying the landing of sand particles and the discontinuity of vegetation, a discrete model may be more suitable. Discrete models can use discrete event systems to describe the state changes of sand particles and vegetation, including the movement of sand, landing, and the frequency of sand impact on vegetation. We will also focus on studying discrete models of vegetative-sand on networks [48, 49].

Use of AI tools declaration

The authors declare they have not used Artificial Intelligence (AI) tools in the creation of this article.

Acknowledgments

The work is supported by the National Natural Science Foundation of China (61872227, 12061081

Conflict of interest

The authors declare there is no conflict of interest.

References

1. UNCED, The United Nations conference on environment and development, 1992.
2. A. J. Bach, Assessing conditions leading to severe wind erosion in the Antelope Valley, California, 1990–1991, *Prof. Geogr.*, **50** (2010), 87–97. https://doi.org/10.1111/00330124.00106
3. J. Leys, G. Mctainsh, Soil loss and nutrient decline by wind erosion-cause for concern, *Aust. J. Soil Water Conserv.*, **7** (1994), p30–35.
4. D. P. C. Peters, K. M. Havstad, Nonlinear dynamics in arid and semi-arid systems: Interactions among drivers and processes across scales, *J. Arid Environ.*, **65** (2006), 196–206. https://doi.org/10.1016/j.jaridenv.2005.05.010
5. D. D. Breshears, J. J. Whicker, M. P. Johansen, J. E. Pinder, Wind and water erosion and transport in semi-arid shrubland, grassland and forest ecosystems: quantifying dominance of horizontal wind-driven transport, *Earth Surf. Processes Landf.*, **28** (2003), 1189–1209. https://doi.org/10.1002/esp.1034
6. J. F. Weltzin, M. E. Loik, S. Schwinning, D. G. William, P. A. Fay, B. M. Haddad, et al., Assessing the response of terrestrial ecosystems to potential changes in precipitation, *BioScience*, **53** (2003), 941–952. https://doi.org/10.1641/0006-3568(2003)053[0941:ATROTE]2.0.CO;2
7. N. English, J. Weltzin, A. Fravolini, L. Thomas, D. G. Williams, The influence of soil texture and vegetation on soil moisture under rainout shelters in a semi-desert grassland, *J. Arid Environ.*, **63** (2005), 324–343. https://doi.org/10.1016/j.jaridenv.2005.03.013
8. G. H. Guo, J. J. Wang, Pattern formation and qualitative analysis for a vegetation-water model with diffusion, *Nonlinear Anal. Real World Appl.*, **76** (2024), 104008. https://doi.org/10.1016/j.nonrwa.2023.104008
9. G. H. Guo, S. H. Zhao, J. J. Wang, Y. X. Gao, Positive steady-state solutions for a water-vegetation model with the infiltration feedback effect, *Discrete Contin. Dyn. Syst. B*, **29** (2023), 426–458. https://doi.org/10.3934/dcdsb.2023101
10. G. H. Guo, Q. J. Qin, D. F. Pang, Y. H. Su, Positive steady-state solutions for a vegetation-water model with saturated water absorption, *Commun. Nonlinear Sci. Numer. Simul.*, **131** (2024), 107802. https://doi.org/10.1016/j.cnsns.2023.107802
11. R. Bastiaansen, M. Chirilus-Bruckner, A. Doelman, Pulse solutions for an extended Klausmeier model with spatially varying coefficients, *SIAM J. Appl. Dyn. Syst.*, **19** (2020), 1–57. https://doi.org/10.1137/19M1255665
12. C. A. Klausmeier, Regular and irregular patterns in semiarid vegetation, *Science*, **284** (1999), 1826-1828. https://doi.org/10.1126/science.284.5421.1826
13. E. Meron, E. Gilad, J. Von Hardenberg, M. Shachak, Y. Zarmi, Vegetation patterns along a rainfall gradient, *Chaos Soliton. Fract.*, **19** (2004), 367–376. https://doi.org/10.1016/S0960-0779(03)00049-3
14. G. McTainsh, C. Strong, The role of aeolian dust in ecosystems, *Geomorphology*, **89** (2006), 39–54. https://doi.org/10.1016/j.geomorph.2006.07.028

15. P. P. Hesse, L. R. Simpson, Variable vegetation cover and episodic sand movement on longitudinal desert sand dunes, *Geomorphology*, **81** (2006), 276–291. https://doi.org/10.1016/j.geomorph.2006.04.012

16. K. Burri, C. Gromke, M. Lehning, F. Graf, Aeolian sediment transport over vegetation canopies: A wind tunnel study with live plants, *Aeolian Res.*, **3** (2011), 205–213. https://doi.org/10.1016/j.aeolia.2011.01.003

17. Y. C. Yan, X. L. Xu, X. P. Xin, G. X. Yang, X. Wang, R. Yan, et al., Effect of vegetation coverage on aeolian dust accumulation in a semiarid steppe of northern China, *Catena*, **87** (2011), 351–356. https://doi.org/10.1016/j.catena.2011.07.002

18. F. F. Zhang, L. Yao, W. J. Zhou, Q. J. You, H. Y. Zhang, Using shannon entropy and contagion index to interpret pattern self-organization in a dynamic vegetation-sand model, *IEEE Access*, **8** (2020), 17221–17230. https://doi.org/10.1109/ACCESS.2020.2968242

19. F. F. Zhang, Y. X. Li, Y. L. Zhao, Z. Liu, Vegetation pattern formation and transition caused by cross-diffusion in a modified vegetation-sand model, *Int. J. Bifurcat. Chaos*, **32** (2022), 2250069. https://doi.org/10.1142/S0218127422500699

20. F. F. Zhang, H. Y. Zhang, M. R. Evans, T. Huang, Vegetation patterns generated by a wind driven sand-vegetation system in arid and semi-arid areas, *Ecol. Complex.*, **31** (2017), 21–33. https://doi.org/10.1016/j.ecocom.2017.02.005

21. M. Alfaro, H. Izuhara, M. Mimura, On a nonlocal system for vegetation in drylands, *J. Math. Biol.*, **77** (2018), 1761–1793. https://doi.org/10.1007/s00285-018-1215-0

22. L. Eigentler, J. A. Sherratt, Analysis of a model for banded vegetation patterns in semi-arid environments with nonlocal dispersal, *J. Math. Biol.*, **7** (2018), 739–763. https://doi.org/10.1007/s00285-018-1233-y

23. Y. Maimaiti, W. B. Yang, J. H. Wu, Turing instability and coexistence in an extended Klausmeier model with nonlocal grazing, *Nonlinear Anal. Real World Appl.*, **64** (2022), 103443. https://doi.org/10.1016/j.nonrwa.2021.103443

24. E. Siero, Nonlocal grazing in patterned ecosystems, *J. Theor. Biol.*, **436** (2018), 64–71. https://doi.org/10.1016/j.jtbi.2017.10.001

25. S. Zaytseva, L. B. Shaw, J. P. Shi, M. L. Kirwan, R. N. Lipcius, Pattern formation in marsh ecosystems modeled through the interaction of marsh vegetation, mussels and sediment, *J. Theor. Biol.*, **543** (2022), 111102. https://doi.org/10.1016/j.jtbi.2022.111102

26. C. H. Zeng, H. Wang, Noise and large time delay: Accelerated catastrophic regime shifts in ecosystems, *Ecol. Model.*, **233** (2012), 52–58. https://doi.org/10.1016/j.ecolmodel.2012.03.025

27. L.F. Lafuerza, R. Toral, Exact solution of a stochastic protein dynamics model with delayed degradation, *Phys. Rev. E*, **84** (2011), 051121. https://doi.org/10.1103/PhysRevE.84.051121

28. S. L. Pan, Q. M. Zhang, T. Kang, A. Meyer-Baese, X. Li, Finite-time stability of a stochastic tree-grass-water-nitrogen system with impulsive and time-varying delay, *Int. J. Biomath.*, **17** (2023), 2350052. https://doi.org/10.1142/S1793524523500523

29. Q. L. Han, T. Yang, C. H. Zeng, H. Wang, Z. Liu, Y. Fu, et al., Impact of time delays on stochastic resonance in an ecological system describing vegetation, *Physica A*, **408** (2014), 96–105. https://doi.org/10.1016/j.physa.2014.04.015

30. J. Li, G. Q. Sun, Z. Jin, Interactions of time delay and spatial diffusion induce the periodic oscillation of the vegetation system, *Discrete Contin. Dyn. Syst. Ser. B*, **27** (2022), 2147–2172. https://doi.org/10.3934/dcdsb.2021127

31. N. F. Britton, Spatial structures and periodic travelling waves in an integro-differential reaction-diffusion population model, *SIAM J. Appl. Math.*, **50** (1990), 1663–1688. https://doi.org/10.1137/0150099

32. H. Wang, On the existence of traveling waves for delayed reaction-diffusion equations, *J. Differ. Equ.*, **247** (2015), 887–905. https://doi.org/10.1016/j.jde.2009.04.002

33. G. Y. Lue, M. X. Wang, Stability of planar waves in reaction-diffusion system, *Sci. China Math.*, **54** (2011), 1403–1419. https://doi.org/10.1007/s11425-011-4210-0

34. M. D. Burlica, D. Rosu, I. I. Vrabie, Abstract reaction-diffusion systems with nonlocal initial conditions, **Nonlinear Anal-Theor.** , **94** (2014), 107–119. https://doi.org/10.1016/j.na.2013.07.033

35. G. F. Webb, A reaction-diffusion model for a deterministic diffusive epidemic, *J. Math. Anal. Appl.*, **84** (1981), 150–161. https://doi.org/10.1016/0022-247X(81)90156-6

36. S. J. Guo, S. Z. Li, On the stability of reaction-diffusion models with nonlocal delay effect and nonlinear boundary condition, *Appl. Math. Lett.*, **103** (2020), 106197. https://doi.org/10.1016/j.aml.2019.106197

37. M. Aguerrea, G. Valenzuela, On the minimal speed of traveling waves for a nonlocal delayed reaction-diffusion equation, *Nonlinear Oscil.*, **13** (2010), 1–9. https://doi.org/10.1007/s11072-010-0096-y

38. Q. Xue, G. Q. Sun, C. Liu, Z. G. Guo, Z. Jin, Y. P. Wu, et al., Spatiotemporal dynamics of a vegetation model with nonlocal delay in semi-arid environment, *Nonlinear Dyn.*, **99** (2020), 3407–3420. https://doi.org/10.1007/s11071-020-05486-w

39. C. Liu, F. G. Wang, Q. Xue, L. Li, Z. Wang, Pattern formation of a spatial vegetation system with root hydrotropism, *Appl. Math. Comput.*, **420** (2022), 126913. https://doi.org/10.1016/j.amc.2021.126913

40. Q. Xue, C. Liu, L. Li, G.Q. Sun, Z. Wang, Interactions of diffusion and nonlocal delay give rise to vegetation patterns in semi-arid environments, *Appl. Math. Computation*, **399** (2021), 126038. https://doi.org/10.1016/j.amc.2021.126038

41. S. J. GUO, Stability and bifurcation in a reaction-diffusion model with nonlocal delay effect, *J. Differ. Equ.*, **259** (2015), 1409–1448. https://doi.org/10.1016/j.jde.2015.03.006

42. C. H. Wang, H. Wang, S. L. Yuan, Precipitation governing vegetation patterns in an arid or semi-arid environment, *J. Math. Biol.*, **87** (2023), 22. https://doi.org/10.1007/s00285-023-01954-0

43. L. Eigentler, J. A. Sherratt, An integrodifference model for vegetation patterns in semi-arid environments with seasonality, *J. Math. Biol.*, **81** (2020), 875–904. https://doi.org/10.1007/s00285-020-01530-w

44. Z. L. Zhen, J. D. Wei, J. B. Zhou, L. X. Tian, Wave propagation in a nonlocal diffusion epidemic model with nonlocal delayed effects, *Appl. Math. Comput.*, **339** (2018), 15–37. https://doi.org/10.1016/j.amc.2018.07.007

45. S. A. Gourley, S. JWH, Dynamics of a food-limited population model incorporating nonlocal delays on a finite domain, *J. Math. Biol.*, **44** (2002), 49–78. https://doi.org/10.1007/s002850100109

46. G. Q. Sun, C. H. Wang, Z. Y. Wu, Pattern dynamics of a Gierer-Meinhardt model with spatial effects, *Nonlinear Dyn.*, **88** (2017), 1385–1396. https://doi.org/10.1007/s11071-016-3317-9

47. Y. L. Song, R. Yang, G. Q. Sun, Pattern dynamics in a Gierer-Meinhardt model with a saturating term, *Appl. Math. Model.*, **46** (2017), 476–491. https://doi.org/10.1016/j.apm.2017.01.081

48. C. Liu, L. L. Chang, Y. Huang, Z. Wang, Turing patterns in a predator-prey model on complex networks, *Nonlinear Dyn.*, **99** (2020), 3313–3322. https://doi.org/10.1007/s11071-019-05460-1

49. J. Y. Zhou, Y. Ye, A. Arenas, S. Gomz, Y. Zhao, Pattern formation and bifurcation analysis of delay induced fractional-order epidemic spreading on networks, *Chaos, Soliton. Fract.*, **174** (2023), 113805. https://doi.org/10.1016/j.chaos.2023.113805

AIMS Press